

AD-A174 521

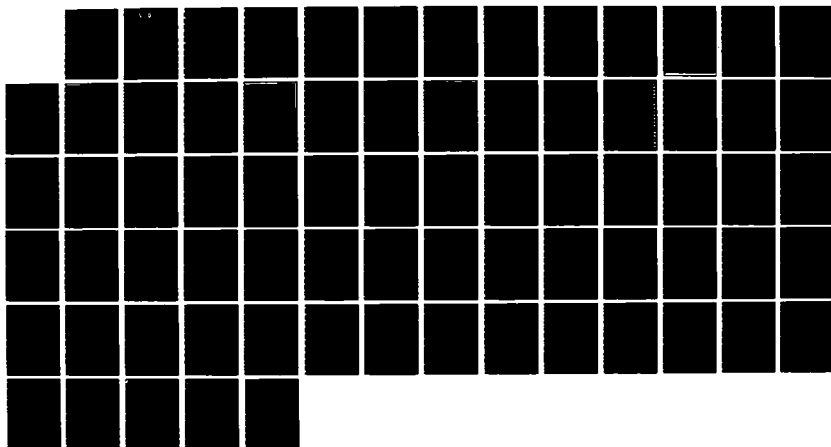
HIGH POWER MILLIMETER-WAVELENGTH COHERENT RADIATION
SOURCES(U) DARTMOUTH COLL HANOVER N H DEPT OF PHYSICS
AND ASTRONOMY J E WALSH 25 SEP 86 86-0168
AFOSR-TR-86-1089 AFOSR-82-0168

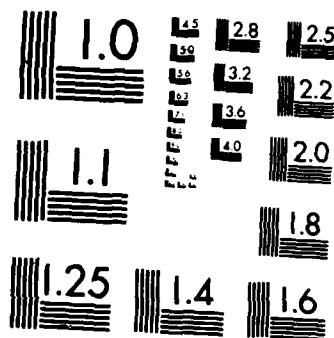
1/1

UNCLASSIFIED

F/G 20/5

NL





MICROCOPY RESOLUTION TEST CHART
NATIONAL BUREAU OF STANDARDS-1963-A

AD-A174 521

DTIC
ELECTE
NOV 26 1986
S D

AFOSR-TR- 86-1089

2

HIGH-POWER,

MILLIMETER-WAVELENGTH, COHERENT

RADIATION SOURCES

FINAL REPORT FOR U.S./A.F.O.S.R. CONTRACT

82-0168

2/1/82 - 1/31/86

AIR FORCE OFFICE OF SCIENTIFIC RESEARCH (AFSR)
NOTICE OF TRANSFER TO DTIC
This technical report has been reviewed and is
approved for public release in accordance with AFM 190-12.
Distribution is unlimited.

Approved for public release;
distribution unlimited.

MATTHEW J. KEEPER
Chief, Technical Information Division

John E. Walsh

Department of Physics and Astronomy

Dartmouth College

Hanover, N.H. 03755

DTIC FILE COPY

DISTRIBUTION STATEMENT A

Approved for public release
Distribution Unlimited

86 11 26 056

UNCLASSIFIED

SECURITY CLASSIFICATION OF THIS PAGE

REPORT DOCUMENTATION PAGE

1a. REPORT SECURITY CLASSIFICATION N/A		1b. RESTRICTIVE MARKINGS	
2a. SECURITY CLASSIFICATION AUTHORITY N/A		3. DISTRIBUTION/AVAILABILITY OF REPORT Unlimited Approved for public release, distribution unlimited	
2b. DECLASSIFICATION/DOWNGRADING SCHEDULE N/A			
4. PERFORMING ORGANIZATION REPORT NUMBER(S)		5. MONITORING ORGANIZATION REPORT NUMBER(S) AFOSR-TR-86-1089	
6a. NAME OF PERFORMING ORGANIZATION Dartmouth College	6b. OFFICE SYMBOL (If applicable)	7a. NAME OF MONITORING ORGANIZATION AFOSR	
6c. ADDRESS (City, State and ZIP Code) Trustees of Dartmouth College Office of Grants & Contracts P.O. Box 7, Hanover, N.H. 03755		7b. ADDRESS (City, State and ZIP Code) Dept. of the Air Force Building 410 Bolling AFB, Washington, D.C. 20332	
8a. NAME OF FUNDING/SPONSORING ORGANIZATION U.S.A.F.O.S.R.	8b. OFFICE SYMBOL (If applicable) NP	9. PROCUREMENT INSTRUMENT IDENTIFICATION NUMBER AFOSR-82-C16E	
8c. ADDRESS (City, State and ZIP Code) AFOSR Building 410, Bolling AFB, D.C. 20332		10. SOURCE OF FUNDING NOS.	
		PROGRAM ELEMENT NO. 61102F	PROJECT NO. 2301
		TASK NO. AB	WORK UNIT NO.
11. TITLE (Include Security Classification) High-Power, Millimeter-Wavelength, Coherent Radiation			
12. PERSONAL AUTHOR(S) Sources/Unclassified John Walsh			
13a. TYPE OF REPORT Final	13b. TIME COVERED FROM 2/1/82 TO 1/31/86	14. DATE OF REPORT (Yr., Mo., Day) 1986, September 25	15. PAGE COUNT 72
16. SUPPLEMENTARY NOTATION			
17. COSATI CODES		18. SUBJECT TERMS (Continue on reverse if necessary and identify by block number)	
FIELD	GROUP	SUB. GR.	
		Cerenkov Maser development; high-power submillimeter radiation sources	
19. ABSTRACT (Continue on reverse if necessary and identify by block number)			
<p>A summary of the results of the Cerenkov Maser development is presented. During the course of this work, operation over the spectral range extending from just below 30 GHz to just above 300 GHz was demonstrated. Sources based upon high-power microwave-tube technology and sources driven by pulse-power generators were both used to drive Cerenkov Masers. In the former type, 10% efficiency from single-pass, untapered resonators were obtained, while in the latter, efficiency was in the 0.1-1% range. Extensive computer codes describing linear and nonlinear aspects of Cerenkov Maser operation were also developed.</p>			
20. DISTRIBUTION/AVAILABILITY OF ABSTRACT UNCLASSIFIED/UNLIMITED <input checked="" type="checkbox"/> SAME AS RPT <input checked="" type="checkbox"/> OTIC USERS <input type="checkbox"/>		21. ABSTRACT SECURITY CLASSIFICATION Unclassified	
22a. NAME OF RESPONSIBLE INDIVIDUAL DR. ROBERT S. BARKER		22b. TELEPHONE NUMBER (Include Area Code) 202/767-5211	22c. OFFICE SYMBOL NP

DD FORM 1473, 83 APR

EDITION OF 1 JAN 73 IS OBSOLETE.

UNCLASSIFIED
SECURITY CLASSIFICATION OF THIS PAGE

CONTENTS

1. Introduction and Summary
2. Degrees Earned with Support of AFOSR
3. Published Work
 - 3.1 The Cerenkov Maser at Millimeter Wavelengths
 - 3.2 The General Aspects of Cerenkov Masers
4. Abstracts of Work Presented at Scientific Meetings

Accession For	
NTIS CRA&I	<input checked="checked" type="checkbox"/>
DTIC TAB	<input type="checkbox"/>
Unannounced	<input type="checkbox"/>
Justification	
By	
Distribution /	
Availability Codes	
Dist	Avail and/or Special
A-1	



1. Introduction and Summary

The principal focus of the four-year program (2/1/82 - 1/31/86) was the development of the Cerenkov Maser. A widely-tunable, high-power, mm-wavelength source was desired, and these characteristics were demonstrated. The experimental effort was concentrated on the development of oscillators, and detailed theoretical studies of both oscillator and amplifier operation were completed.

The oscillator experiments were undertaken with two types of beam generator. The first was based on conventional high-power microwave-tube technology. A pulse-transformer was driven by a pulse-forming network which was discharged by a hydrogen thyratron. Typical operating parameters were $V_b = 100\text{-}200$ KV, with 2-20 A of current. Operation over the entire range from 1 cm to 1 mm was achieved. In the 1 cm - 5 mm region, multi-hundreds of KW were obtained which implied single-pass, untapered efficiencies in the 10% range. At 3 mm, the power level was approximately 100 KW, and a few KW were observed at frequencies as high as 300 GHz.

A second series of experiments was conducted with a beam formed by a pulse-power generator. The beam was produced on a cold cathode which terminated a Marx-capacitor-configuration-driven transmission line. Operation between 150 and 315 GHz was demonstrated and tuning of a single resonator from 190 to 315 GHz was observed. At the long-wavelength end of this region power output was conservatively estimated to be 500 KW and at

the shorter end, the levels were in the multi-ten's of KW range.

Below 150 GHz, the pulse-transformer-driven Cerenkov Maser operated on the fundamental TM_{01} mode of a cylindrical dielectric-lined waveguide. In order to compare observed behavior with theoretical expectation, extensive development of computer codes for predicting the tuning characteristics and the gain of these structures was also undertaken. The cylindrical structures were convenient for mm-wavelength oscillator operation, but at shorter wavelengths (submm - FIR) and for amplifier operation, planar structures have some advantages. The latter were not given extensive experimental tests during the course of this project, but the theoretical characterization was completed. Gain and saturation of Cerenkov amplifiers was computed and in the longer-wavelength end of the mm range, 10-30 db of gain can be obtained from structures of moderate length (10-20 cm).

Also completed were two sub-projects on the nonlinear aspects of the Cerenkov Maser. In one, the saturation of the instability was investigated and in the other, the possibility of mode-locked operation was investigated. The results of the first calculations gave output power, predictions which were generally in accord with experimental observations. During the second work, the mode-locked operation of a spectrum of plasma modes was demonstrated and evidence was found for natural mode-locking of shorter-wavelength Cerenkov oscillations (in the 2-1 mm range). Abstracts of the doctoral dissertations in which this work is described are contained in Section 2 of this report.

In general, it was demonstrated that Cerenkov sources are a viable source of coherent, tunable, high-power radiation in the mm region of the spectrum. They could have application in many areas such as extremely intense source development, or high-power radar or electronic warfare. In the remaining sections of this report, more detailed summaries of published work and abstracts of work presented at meetings are included. Copies of the publications and the dissertations are available from the Dartmouth College Plasma Physics Library.

2. Degrees earned with the Support of AFOSR Contract 82-0168.

In this section, a list of titles and abstracts of theses completed with the support of this contract, are included.

Copies of all theses are available from:

Dartmouth College
Plasma Laboratory
Physics Department
Wilder Hall
Hanover, N.H. 03755

1. S. Von Laven, Ph.D. (1982).
2. L. Wiencke, A.B. Honors (1983).
3. J. Branscum, A.M. (1984).
4. J. Murphy, Ph.D. (1982).
5. M. Abdelkarim, Ph.D. (1984).
6. T. Buller, Ph.D. (1985).
7. B. Johnson, Ph.D. (1985).
8. E. Garate, Ph.D. (1985).
9. R. McCowan, Ph.D., (1986).

Characterization of a Cerenkov Maser

* * *

Submitted in partial fulfillment of
the requirements for the degree
of Doctor of Philosophy

* * *

Dartmouth College
Hanover, N.H. 03755
April, 1982

Scott Von Laven

ABSTRACT

The interaction of a magnetized electron beam with a slow guided electromagnetic wave has been studied experimentally. An electron beam driven, dielectric-lined, cylindrical waveguide has produced 30-100 kilowatts of coherent radiation over an octave band on the TM_{01} mode of the waveguide. Operation on the TM_{02} mode has been realized as well. Impedance mismatches at the ends of the liner section provide a reflected signal, which undergoes amplification during successive passes.

The growth rate of the interaction is calculated, taking into account the cylindrical geometry of the experiment, for the collective regime and for the single particle regime. An estimate of the saturating field amplitude leads to predicted powers for comparison with experiments.

CERENKOV FREE ELECTRON LASERS IN THE INFRARED

A Thesis

Submitted to the Faculty
in partial fulfillment of the requirements for the
degree of

Doctor of Philosophy

by

James Brian Murphy

Dartmouth College

Hanover, New Hampshire 03755

June 1982

Examining Committee:

W. F. E. Hall
Chairman

Agnes Fyffe
Christine M. Alata
Richard L. Smith

Dwight Lahr
Dean of Graduate Studies

ABSTRACT

We evaluate the Cerenkov free electron laser (CFEL) as a potential infrared radiation source. The model we consider consists of a relativistic electron beam grazing the surface of a single slab dielectric waveguide. Properties of the resonator such as transverse mode spacing, scaling of the output frequency with slab thickness and dielectric constant are examined. We find the single slab waveguide, with a thickness on the order of the output wavelength, operating in the TM1 mode, to be a suitable choice as a resonator for a CFEL.

The small signal gain of the device is computed for the single particle interaction mechanism for the cases of an infinite and zero magnetic guide field. An examination of the expression for the gain shows it to be independent of the dielectric material for operation in the infrared regime. Although a low dielectric constant ($\epsilon \sim 2-4$) is desirable as it provides for thicker waveguides capable of handling higher power outputs. In the mm regime the gain of the CFEL is enhanced by using materials with moderately high dielectric constants ($\epsilon \sim 10-25$).

We compared the small signal gain of the CFEL to that of an undulator device. If one requires the CFEL to use same high energy beams ($\gamma \sim 10-80$) as the undulator device, the undulator offers higher gain. The Cerenkov device has

the advantage that it can operate at a desired frequency with a lower energy beam. When this fact is taken into account the CFEL is the more attractive device.

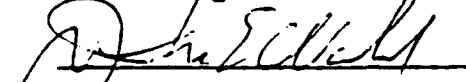
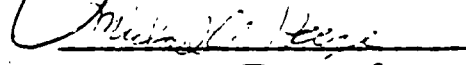
We estimate the nonlinear saturation based on a particle trapping model. The losses in the dielectric are assessed and found not to be prohibitively large. We conclude that operation of a CFEL in the infrared portion of the spectrum is a realistic possibility.

QUASI-OPTICAL TECHNIQUES
AT
MILLIMETER AND SUBMILLIMETER WAVELENGTHS

A Thesis
Submitted in Partial Fulfillment of the
Requirements for the Honors Major

by
Lawrence R. Wiencke
DARTMOUTH COLLEGE
Hanover, New Hampshire
June, 1983

Examining Committee:



W.T. Doyle

Abstract

At millimeter and submillimeter wavelengths quasi-optical techniques are useful and practical. This thesis, the result of research done in the Dartmouth College Plasma Laboratory, contains descriptions and analysis of several quasi-optical devices, which were constructed as diagnostics for a Cerenkov Free Electron Laser, as well as simply for their own development.

The prism directional coupler, and the prism multiplexer, based on the principal of frustrated internal reflection, exhibited a bandwidth, and power handling capability far greater than that of conventional components. It appears that power and frequency measurements in the kilowatt range at millimeter wavelengths could be made using these devices. The directional coupler was used as a diagnostic on the Cerenkov FEL with good results.

Several parallel plate Fabry Perot interferometers were also investigated, an interferograms indicating 97 ghz output from the Cerenkov FEL were obtained.

The prism coupled slab waveguide resonator, like the directional coupler and multiplexer, was based on the principle of frustrated internal reflection. This device, having possible applications as a maser, a diagnostic instrument, and spectroscopic instrument, provided an interesting method of studying interactions between millimeter waves and water droplets. Such was its sensitivity, that evaporation rates of water films could be measured.

"NONLINEAR THEORY OF THE CERENKOV MASER"

M. Abdelkarim

Department of Physics & Astronomy
Dartmouth College
Hanover, N.H. 07355

Ph.D. Thesis

November, 1983

A Rectangular, Two-slab Dielectric Resonator
for the Cerenkov FEL

A Thesis

Submitted to the Faculty
in partial fulfillment of the requirements for the
degree of

Master of Arts

by

John Branscum

Dartmouth College

Hanover, New Hampshire 03755

May 1984

Examining Committee:

John E. Wall
Chairman

William C. Smith

Joseph J. B. Davis

Dwight Lahr
Dean of Graduate Studies

Abstract

The field components and the dispersion relations for the two mode types of a partially-filled, rectangular waveguide are found. Using established techniques to describe beam-wave interactions in a slow-wave structure, an electron beam is theoretically introduced into the resonator, and wave growth is described. Output frequency, bandwidth, and gain are considered for a Cerenkov FEL using the rectangular geometry. Finally, it is shown that the rectangular geometry in the Cerenkov FEL does show promise for use as a high-power microwave amplifier.

A Metal-Grating Free-Electron Maser

A Thesis

Submitted to the Faculty

**in partial fulfillment of the requirements for the
degree of**

Doctor of Philosophy

by

Thomas L. Buller

DARTMOUTH COLLEGE

Hanover, New Hampshire

August 1985

ABSTRACT

The development of a class of mildly relativistic electron beam driven open resonator oscillators is summarized. The devices are based on a grating loaded parallel plate waveguide structure which, together with terminating cylindrical mirrors or a cylindrical mirror/horn antenna combination, form an open resonator. Electron beam voltages between 30 and 150 kV and currents between 1 and 20 A have been used to achieve 20-30 kW output levels in the 7 mm wavelength range and approximately 10 kW in the 4 mm region.

Theory describing the operating characteristics of these devices; small signal gain, tuning range, and saturation levels has been developed. We will present a detailed summary of the theory and the results of an extensive series of measurements.

AN INFRARED CERENKOV LASER

A Thesis

Submitted in Partial Fulfillment of the
Requirements for the Doctor of
Philosophy

by

Bernadette Johnson

DARTMOUTH COLLEGE

Hanover, New Hampshire

June, 1985

ABSTRACT

A theoretical examination of the operating characteristics of far infrared wavelength Cerenkov lasers is presented. The basic features of the device are described and the dispersion relations of several dielectric loaded resonators are examined in detail. Emphasis is on planar resonators which support Gaussian quasi-optical modes. It is shown that these are particularly well suited for the operation of electron beam - driven sources at far infrared and shorter wavelengths. Expressions for the electron beam - operating wavelength relation and the small signal gain behavior of these resonators are developed. The nonlinear saturation is examined and the available output power is estimated. A number of practical limitations such as the effect of dielectric loss are explored, and detailed designs for far infrared proof-of-principle experiments are discussed.

Cerenkov Masers at Lower Millimeter Wavelengths

A Thesis

Submitted to the Faculty

in partial fulfillment of the requirements for the
degree of

Doctor of Philosophy

by

Eusebio P. Garate

Dartmouth College

Hanover, New Hampshire 03755

May 1985

Examining Committee:

Chairman

Dean of Graduate Studies

ABSTRACT

A Cerenkov Maser, consisting of a mildly relativistic electron beam and a dielectric lined slow waveguide has produced tunable, coherent radiation of 1-100 KW at wavelengths from 2.5 to 3.75 mm corresponding to beam velocity synchronism with the TM_{01} mode of the waveguide. Operation on higher order waveguide modes at frequencies up to 320 Ghz has produced power levels of 1 watt. Results are reported of a preliminary set of experiments using two stage resonant slow wave structures.

The dispersion relation for the TM_{0n} modes of a partially filled, dielectric lined, cylindrical waveguide driven by a cold, relativistic electron beam is derived, including the effect of a gap between the electron beam and the dielectric liner. The dispersion relation is then used to derive an expression for the growth rate of the Cerenkov instability in the tenuous beam, collective limit. Also presented is an equation for the growth rate in the single particle limit for cylindrical waveguide geometry. Expressions are developed for the minimum current necessary to overcome cavity losses and for the power output of the Cerenkov maser for both the collective and single particle regimes. The results of the calculations for the collective limit are shown to be in good agreement with the laboratory measurements.

"GENERAL NONLINEAR MECHANICS OF AN ELECTRON
BEAM DRIVEN MULTIMODE PLASMA SYSTEM"

Robert B. McCowan

Department of Physics & Astronomy
Dartmouth College
Hanover, N.H. 03755

Ph.D. Thesis

February, 1986

* * *

Abstract

The general nonlinear behavior of the beam driven multimode system is examined. The linearized dispersion for a beam plasma is reviewed and the new features of linear theory needed to explain the behavior for the plasma with two oppositely directed beams are derived.

The dispersion relation and an extension of van der Pol theory are used to develop nonlinear amplitude rate equations for the plasma. Where quantitative comparison is possible agreement between the model and the experimental behavior is within the expected ranges.

Important qualitative features of the nonlinear multimode system, mode locking and entrainment are observed in the model and in the experiment.

An apparatus for experimental test of the model was built. The components of the system included a vacuum vessel, magnets to guide the electron beam and confine the plasma and an electron gun to provide the electron beam. Diagnostics used in the experiment were also built and include probes, a microwave resonance shift cavity and a retarding field energy analyzer. Data were collected and recorded by single channel superheterodyne receivers, spectrum analyzers and a Data Precision D6000, a digital waveform acquisition and analysis system. An Apple Macintosh computer is used to communicate with the D6000 and details of the communications between the D6000 and the Macintosh are also presented.

3. Published Work

This section contains reprints of work published in refereed journals. It is divided into two main groups: work aimed primarily at the potential of Cerenkov devices in the mm-range of the spectrum (entries 1-4), and work pertaining to the more general aspects of Cerenkov devices (entries 5 and 6).

3.1 The Cerenkov Maser at Millimeter Wavelengths.

1. High-Power Cerenkov Maser Oscillator.
2. Cerenkov Maser Operation at Lower-Millimeter Wavelengths.
3. The Cerenkov Maser at Millimeter Wavelengths.
4. Cerenkov Maser Operation at 1-2 Mm Wavelengths.

3.2 General Aspects of Cerenkov Masers.

1. Cerenkov Lasers.
2. Space-Charge-Cerenkov and Cyclotron-Cerenkov Instabilities in an Electron-Beam Dielectric System.

High-power Cerenkov maser oscillator

S. Von Laven, J. Branscum, J. Golub, R. Layman, and J. Walsh
Dartmouth College, Hanover, New Hampshire 03755

(Received 23 April 1982; accepted for publication 22 June 1982)

An electron beam driven dielectric-lined waveguide has produced 30–100 kW of coherent radiation over an octave band on the TM_{01} mode of the waveguide. Operation of the TM_{02} mode has been realized as well. Impedance mismatches at the ends of the liner section provide a reflected signal, which undergoes amplification during successive passes.

PACS numbers: 32.30.Bv, 85.10.Hy, 42.52. + x, 41.70. + t

Recent experimental work in the production of stimulated Cerenkov radiation has upheld predictions with regard to output frequency and determined rough threshold beam parameters.¹ New data demonstrate that high power and wide tunability are obtainable through the Cerenkov interaction.

The Cerenkov radiation that is generated when a beam of charged particles passes at superluminal velocity through

or near a dielectric can, in turn, modulate the beam. Some of the radiation must be constrained to propagate in the volume occupied by the beam. The nature of the beam modulation is an axial bunching, which enhances the intensity of subsequent radiation. Beams of sufficient current density, which are strongly coupled to the radiation field, will achieve a growth rate for this Cerenkov instability sufficient to overcome the various loss mechanisms. Discussion of the theo-

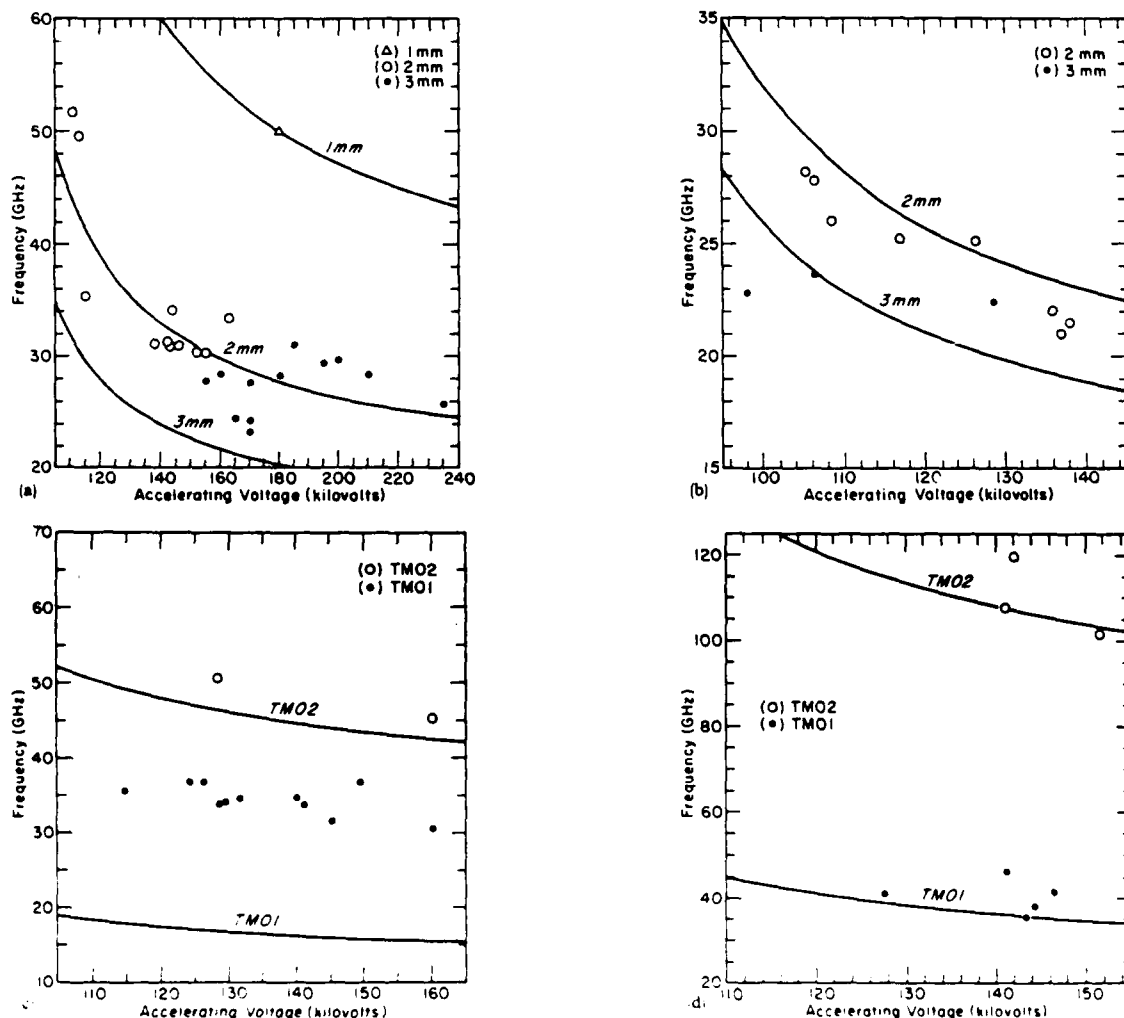


FIG. 1. (a) Frequency of a coupling mode is plotted vs the synchronous beam voltage to give a "tuning curve." The frequency measurements made with quartz liners of 1-, 2-, and 3-mm thicknesses are displayed along with the TM_{01} tuning curves for those liners. The guide diameter, $2b$, is 12.5 mm. (b) Data and TM_{01} tuning curves for 2- and 3-mm-thick boron nitride liners in 12.5-mm guide. (c) TM_{01} and TM_{02} tuning curves and data for a 3-mm stycast liner in 12.5-mm guide. (d) TM_{01} and TM_{02} tuning curves and data for a 1.5-mm boron nitride liner in 9.5-mm guide.

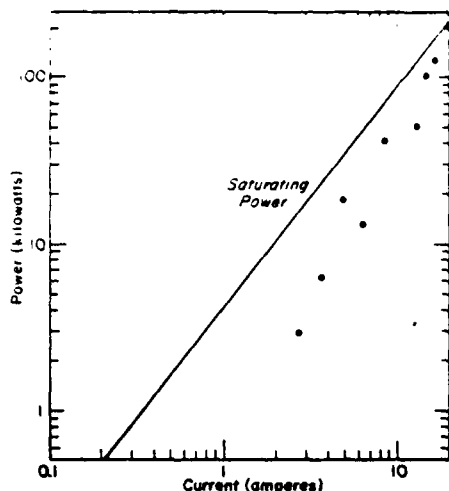


FIG. 2. Saturating power and measurements (+) for 2-mm boron nitride with a 50-keV beam. The saturating power is evaluated assuming a 6-mm beam diameter.

retical background pertaining to this device has been presented earlier.²

The work described here employs a pulsed, 1–40 A beam of 100–250-keV electrons directed along the axis of a dielectric-lined circular waveguide. The pulse duration is about 4 μ s. Design details of the electron beam generator were described in an earlier article.¹

The waveguide geometry is such that the lowest order, azimuthally symmetric, transverse magnetic modes will have a large axial electric field amplitude in the beam volume, even when the phase velocity of the mode is less than c . The strength of the Cerenkov interaction is greatest for phase velocities slightly less than the beam velocity. Since the phase velocity of any of the waveguide modes decreases with increasing frequency, a favorable scaling law is obtained for output frequency with respect to beam energy for a given dielectric liner.

Quartz ($\epsilon = 3.78$), stycast ($\epsilon = 5$), and boron nitride ($\epsilon = 4.2$) liners of several thicknesses have been employed. Frequency measurements are made with a mechanically driven, free space, Fabry-Perot interferometer.³ Power measurements are made with calibrated lengths of a lossy material and either square-law detector diodes or a pyro-electric energy meter.

For almost every dielectric line used, the fundamental output frequency is near the frequency at which the TM_{01} mode is synchronous with the beam. Figures 1(a)–1(c) show the frequencies obtained in a 12.5-mm-diam waveguide. A large systematic offset is noted for the case of the 3-mm quartz liner. A surface charge buildup on the quartz is suspected of decelerating the beam to velocities synchronous with the observed output. The problem nearly disappears for the 2-mm quartz. The longitudinal electric field associated with the 1-mm liner geometry is too weak to give a good coupling for the beam energy employed. At higher voltages and currents which are necessary, the performance of the beam generator is less consistent. Thus, the probability of recording a noise-free interferogram, requiring approxima-

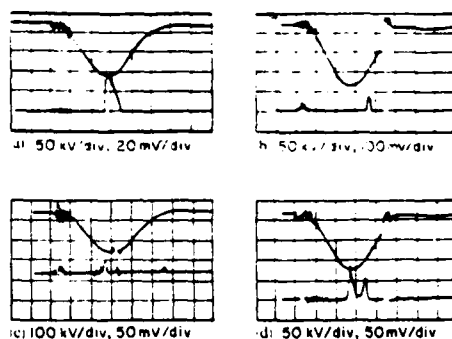


FIG. 3. Microwave output (bottom trace) occurs when the beam velocity (top trace indicates voltage) is synchronous with one of the axial modes of the resonating cavity, not necessarily at the peak beam voltage (1 μ s per division).

tely 1000 shots, is low.

The general behavior of the power as a function of beam current for the 2-mm quartz liner is shown in Fig. 2. In a separate, absolute measurement with the same liner geometry, a 12-A, 115-keV beam generated 30 kW of radiation at 50 GHz. The power is consistent with the power which would be produced by a strongly bunched beam $\{n = n_0 \exp[-i(\omega t - kz)]\}$.⁴ Powers up to 100 kW were obtained at lower frequencies for 3-mm-thick boron nitride in the 12.5-mm-diam waveguide. Power is often sufficient to cause atmospheric breakdown in the X-band waveguide.

The range of frequencies obtainable on a single mode has reached nearly an octave. In some of the 12.5-mm-diam waveguide experiments and in a 9.5-mm waveguide experiment, it has been possible to suppress the TM_{01} mode and observe coupling to the TM_{02} mode [Figs. 1(c) and 1(d)]. Frequencies between 100 and 120 GHz have been attained. The power appears to be less than that obtainable on the TM_{01} mode, but is still significant. Output of still lower apparent power has been observed through a 200-GHz filter with the 2-mm quartz liner 12.5-mm waveguide. All the shorter wavelength power measurements are made with 1-N53 diodes in a Ka band mount. This system is difficult to calibrate when it is far out of band. The voltage response generated at these short wavelengths would have corresponded to one-tenth to one-quarter of the power measured in the 8-mm region, if the wavelengths had been in the design band of the mount. Hence, the shorter wavelengths the output power would, at a minimum, be in the 1-kW range.

The Cerenkov interaction is not continuously tunable within a given band in the present experiment. Signals which undergo longitudinal reflections and make many passes through the liner section of the waveguide without suffering destructive interference reach large amplitude, as in a conventional laser. Thus discrete cavity modes are observed rather than a continuous waveguide spectrum.

Assume that output is generated when the beam is at its peak energy, as in Fig. 3(a). A small increase in the peak energy which is insufficient to reach synchronism with the adjacent longitudinal mode, often leads to output on the original mode. However, the output is now generated when the beam energy is at its original peak value, earlier or later in

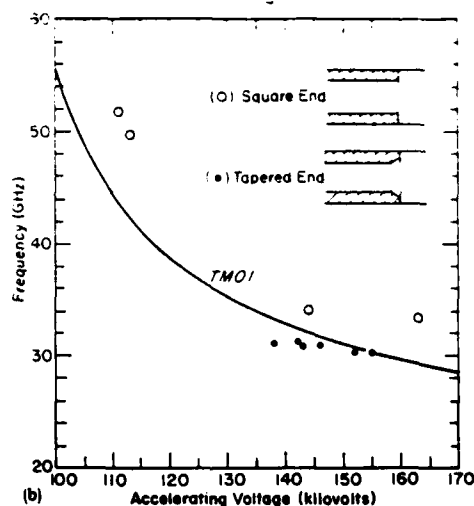
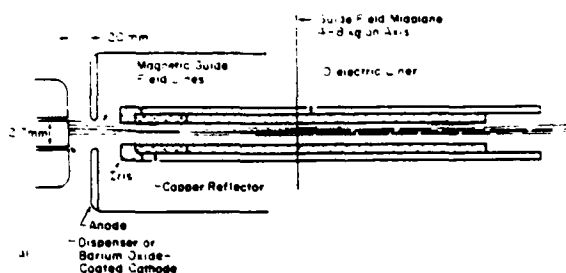


FIG. 4. (a) Cavity formed by the metal-dielectric and vacuum-dielectric interfaces at the ends of the liner section has a sufficient Q for oscillation, given the high gain of the Cerenkov maser. (b) Threshold for oscillation rises for a cavity with lower Q . The lower Q is obtained with a short taper at the downstream end of the liner to reduce the reflected signal.

the pulse than the new peak, or both earlier and later [Figs. 3(b)–3(d)].

If the effective reflectivity at either end of the liner section is reduced, a higher beam voltage threshold is observed. As shown in Fig. 4(a) a copper liner with transverse dimensions identical to the dielectric liner is positioned to act as an upstream mirror. A lower reflectivity downstream is provided by a normal dielectric-vacuum interface. The net reflectivity is reduced by removing the copper liner or by tapering the downstream inner diameter of the dielectric liner outward. The data in Fig. 4(b) indicate the increased threshold due to tapering. A very large current increase could probably substitute for the voltage increase. However, such a current is not available from our present device.

In summary, Cerenkov devices are a potentially useful member of the family of millimeter wave sources. Peak output power at longer wavelengths is comparable to that of other sources, such as gyrotrons,^{5–7} and the peak efficiency (1–10%) is what would be expected for a nonoptimized traveling wave device. It also performs well in the regime where

the wavelength is less than the transverse dimension of the guide. Thus, it also shows promise as a lower millimeter and submillimeter source.

Support by AFOSR contract 82-0168 is acknowledged.

¹K. L. Felch, K. O. Busby, R. W. Layman, D. Kapilow, and J. E. Walsh, *Appl. Phys. Lett.* **38**, 601 (1981).

²J. Walsh, "Stimulated Cerenkov Radiation," in *Advances in Electronics and Electron Physics* (Academic, New York, 1982), Vol. 58.

³D. Wise, Master's thesis, 1981—available from Dartmouth College, Thayer School of Engineering.

⁴S. Von Laven, Ph.D. thesis, 1982—available from Dartmouth College, Physics Department.

⁵R. S. Symons and H. R. Jory, "Cyclotron Resonance Devices," in *Advances in Electronics and Electron Physics* (Academic, New York, 1980), Vol. 55.

⁶J. L. Hirshfield, "Gyrotrons," in *Infrared and Millimeter Waves* (Academic, New York, 1979), Vol. 1.

⁷A. A. Andronov, V. A. Flyagin, A. V. Gapanov, A. L. Gol'denberg, M. I. Petelin, V. G. Usov, and V. K. Yulpatov, *Infr. Phys.* **18**, 385 (1978).

Čerenkov maser operation at lower-mm wavelengths

E. Garate, R. Cook, P. Heim, R. Layman, and J. Walsh

Department of Physics and Astronomy, Dartmouth College, Hanover, New Hampshire 03755

(Received 25 September 1984; accepted for publication 2 April 1985)

The basic operating principles of Čerenkov maser oscillators are briefly reviewed and the experimental performance of a 3-mm device is discussed. A power level of approximately 100 kW was achieved at 88 GHz and voltage tuning from 84 to 128 GHz on the fundamental TM_{01} mode was observed. Operation on higher-order modes at frequencies up to 300–320 GHz was demonstrated, and a two-stage buncher-amplifier configuration was investigated.

I. INTRODUCTION

Previous experimental work^{1,2} on the generation of stimulated Čerenkov radiation has demonstrated the wide tunability and high-power capabilities of the Čerenkov masers at cm wavelengths. In this work, recent experimental results are presented which (1) verify the dependence of output frequency on the transverse geometry of the dielectric liner, (2) demonstrate agreement between the beam threshold parameters and the theoretically predicted and observed threshold for oscillation, and (3) display the wide tunability and high-power capability of the Čerenkov maser in the 3- to 4-mm-wavelength region.

A brief description of the basic features of a Čerenkov maser and a summary of the theoretical results needed to characterize the experiment are presented in the next section. Discussions of the principal experimental results and a conclusion follow.

II. THEORY

The general theory of devices based on stimulated Čerenkov radiation has been discussed previously,^{3,4} and in this section we will present, without derivation, some results needed for interpretation of the experiment. A further detailed discussion of the theory of dielectric-lined relativistic electron-beam-driven waveguides will be presented separately.

Čerenkov radiation is produced when a charged particle traveling at superluminal velocities passes through or near a dielectric medium.⁴⁻⁷ If a resonant structure such as a dielectrically lined waveguide is driven by a relativistic electron beam, the Čerenkov instability causes bunching of the electron beam in the axial component of a TM_{on} mode of the waveguide. The frequency of the radiation produced is determined by the beam velocity and the guide geometry.

The dispersion curve of the TM_{on} modes of a dielectric-lined cylinder have a region where the phase velocity of the mode is less than the speed of light *in vacuo*, and in this region an electron beam can be velocity matched to wave (Fig. 1). In Fig. 1, a conventional plot of angular frequency ω (in units ω/c , c is the speed of light) versus guide wave number k is displayed. The frequency synchronism is determined by the condition $\omega/c k = v_0/c$ (v_0 is the beam velocity). It is also interesting to display this synchronous frequency as a function of beam energy and this is done in Fig. 2. As the beam voltage drops toward the Čerenkov threshold, λ_T^2

$= \epsilon/(\epsilon - 1)$, the synchronous frequency rises rapidly.

In general, smaller transverse liner dimensions or lower dielectric constants yield higher synchronous frequencies for a fixed beam velocity. When the liner dimensions and dielectric constant are fixed, decreasing the beam velocity tunes the synchronous frequency upwards along the dispersion curve. It is also possible to couple higher-order modes of the waveguide, and in this way, very high frequencies can be obtained. However, the growth rate for the higher-order modes will be smaller than that for the fundamental.

It is expected that for the transverse liner dimensions and current densities used in these experiments, the Čerenkov maser is operating in the collective limit. A complete dispersion relation in this regime for the electron-beam-driven TM_{on} mode is found by matching appropriate boundary conditions at the beam-vacuum and vacuum-dielectric interfaces. It can be represented by the expression

$$D[\omega, k, \chi_b(\omega, k)] = 0, \quad (1a)$$

which follows from the application of Maxwell's equations, the Lorentz force equation, the continuity equation, and the previously cited boundary conditions. The function

$$\chi_b \equiv -\frac{1}{4\pi} \frac{\omega_b^2}{\gamma^3} \frac{1}{(\omega - kv_0)^2} \quad (1b)$$

is the beam susceptibility. In writing Eq. (1b), it has been assumed that the beam is guided by a static axial magnetic

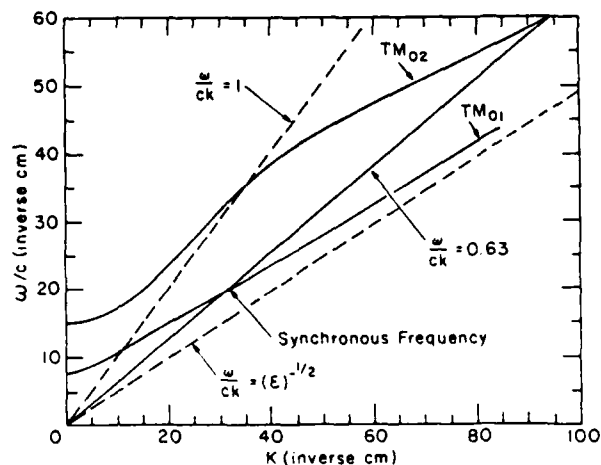


FIG. 1. The dispersion relation of a dielectric-lined waveguide for TM_{01} and TM_{02} waveguide modes. The synchronous frequency is shown for a 150 kV electron beam.

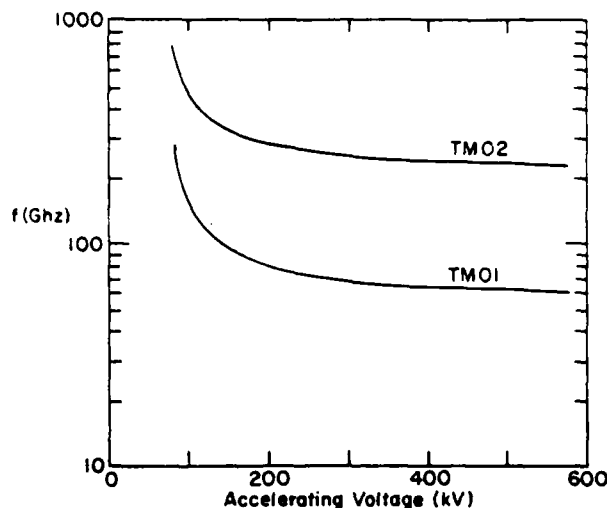


FIG. 2. The tuning curve for the TM_{01} and TM_{02} modes of a 1/2-mm-thick boron nitride-lined waveguide. The inner radius of the dielectric liner is 0.24 cm, and the current = 10 A.

field, which is strong enough to render the electron motion one dimensional. It should also be noted that the susceptibility is linear in the square of the beam plasma frequency

$$\omega_b^2 = \frac{4\pi n e^2}{m} \quad (1c)$$

(n_0 = the peak beam density, e = the electronic charge, m = the electron rest mass), and depends inversely on the cube of γ , the relative energy ($\gamma = 1/\sqrt{1 - v_0^2/c^2}$).

Equation (1) is a complicated transcendental function which, in addition to the variables mentioned, also explicitly depends on the geometric parameters of the guide and the beam. In the absence of the beam, the roots of the function

$$D^{(0)}(\omega, k) \equiv D(\omega, k, 0)$$

determine the empty guide dispersion curves which are displayed in Figs. 1 and 2.

A useful representation of the dispersion relation of the driven system can thus be obtained by first expanding the complete expression around χ_b :

$$D = D^{(0)} + \frac{\partial D}{\partial \chi_b} \bigg|_{\chi_b=0} \chi_b, \quad (2a)$$

and then subsequently around the roots of $D^{(0)}$:

$$\omega = \pm \omega_k.$$

The resulting expression has the form

$$D = (\omega - \omega_k) \frac{\partial D^{(0)}}{\partial \omega} \bigg|_{\omega=\omega_k} + \frac{\partial D}{\partial \chi} \bigg|_{\chi_b=0, \omega=\omega_k} \chi_b, \quad (2b)$$

where $D^{(0)}(\omega_k, k) \equiv 0$, by definition. The second term in Eq. (2b) will be dominated by the double pole in χ_b and the gain [the imaginary part of the root of Eq. (2b)] will peak near

$$kv_0 = \omega.$$

Defining

$$\Delta = \omega - kv_0,$$

$$= \omega - \omega_k,$$

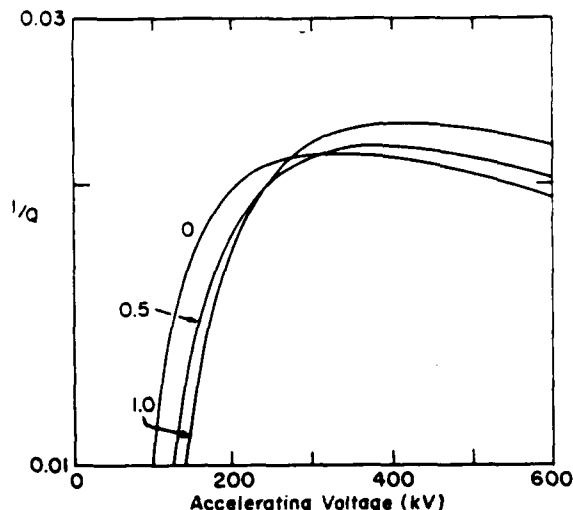


FIG. 3. The relative growth rate for the TM_{01} mode of a 1/2-mm-thick boron nitride liner with dimensions of Fig. 2. The beam-dielectric gap is the parameter.

an expression for the complex frequency shift

$$\Delta^3 = \frac{\partial D / \partial \chi \big|_{\chi_b=0}}{\partial D^{(0)} / \partial \omega \big|_{\omega=\omega_k}} \frac{\omega_b^2}{\gamma^3} \quad (3)$$

is obtained. The right-hand side of Eq. (3) contains all of the relevant kinematic and geometric information. When displayed as a function of beam voltage, it will rise rapidly near the Čerenkov threshold, reach a relative maximum at voltages between 2 and 3 times the threshold, and then decrease slowly as beam energy is further increased. The numerator of the first group of terms will also depend upon the gap between the beam and the dielectric. As the gap increases, measured in units of $\text{gap}/\lambda\beta\gamma$, the growth rate decreases.

It will be convenient in the discussion of the experiment

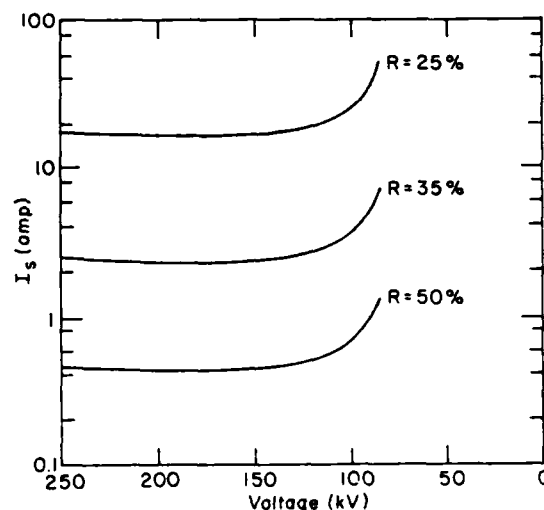


FIG. 4. The current necessary for oscillation threshold. The reflectivities are $R = 0.25, 0.35, 0.50$. The beam-dielectric gap is zero. The liner dimensions are those of Fig. 2.

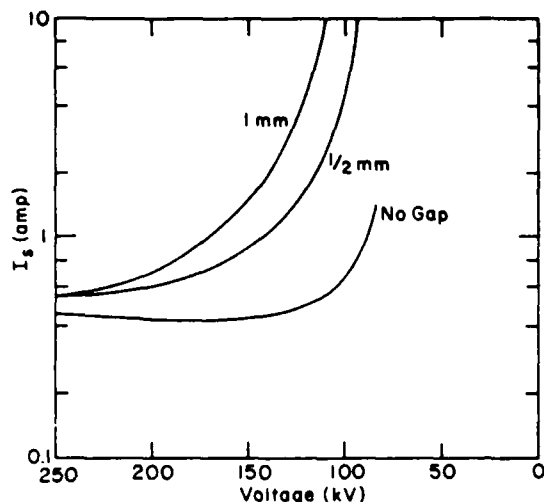


FIG. 5. The current necessary for oscillation threshold. Beam-dielectric gaps are 0, 0.5, and 1 mm and a reflectivity of $R = 0.5$ is assumed. The liner dimensions are those of Fig. 2.

to introduce one further definition:

$$\frac{1}{Q_b} \equiv \frac{I_m \Delta}{\omega}, \quad (4)$$

which is an expression of the relative growth rate in a dimensionless form. It is displayed in Fig. 3. In the figure, the transverse liner dimensions correspond to synchronous frequency of 100 GHz on the TM_{01} mode at a beam voltage of 150 kV. The relative growth rate for these linear dimensions peaks between 150–200 kV. Note that an increase in the beam-dielectric gap (relative to output wavelength) results in the expected decrease in the relative growth rate. The relative growth rate also decreases rapidly near the threshold voltage, since in this limit the output wavelength λ also decreases rapidly and the beam-field coupling cannot be maintained, i.e., the $gap/\lambda\beta\gamma$ becomes large in this limit. Finally, it should be noted that the crossing of the $1/Q_b$ curves results from holding the current constant as the gap is increased.

The maximum growth rate for the TM_{02} mode of the

partially filled guide is approximately one half that of the TM_{01} mode. A more significant beam-mode decoupling occurs for small beam-dielectric gaps on the TM_{02} mode since the output wavelength is much shorter and the coupling cannot be maintained at small accelerating voltages.

Using the expression for growth rate, it is possible to calculate the minimum current needed to overcome cavity losses. Oscillation threshold will occur when

$$\frac{1}{Q_b} > \frac{1}{Q_L},$$

where Q_L is the loaded Q of the cavity. Assuming losses in the active region are small, we can set

$$Q_L = \frac{4\pi L}{\lambda} \frac{R^2}{1 - R^2},$$

where L is the cavity length and R is the reflectivity of the output coupling transition.

Figures 4 and 5 indicate the threshold current needed to overcome cavity losses for liner dimensions typical of those used in the experiments. Again, the important feature is the rapid increase in the threshold current needed as the beam-dielectric gap increases and the exponential increase in start currents near threshold. However, for cavity reflectivities in the 0.1–0.5 range and relatively small beam-dielectric gaps (0.1–0.5 mm), the threshold current needed to overcome cavity losses are modest.

III. EXPERIMENTAL RESULTS

A schematic diagram of the electron beam generator and resonator structure is shown in Fig. 6. The cathode used in these experiments is barium-oxide coated and produces current densities of about 10 A/cm². The output voltage pulse can be varied from 0 to –300 kV. It is 2 μ s wide at the peak voltage and typical repetition rate is 10 Hz. The electron beam is accelerated from the cathode through a hole in the molybdenum anode and into the boron nitride-lined waveguide. An axial magnetic guide field, whose strength can be varied between 2.5 and 8 kG, guides the beam through the interaction region. As the electron beam emerges from the lined waveguide it follows diverging magnetic field lines

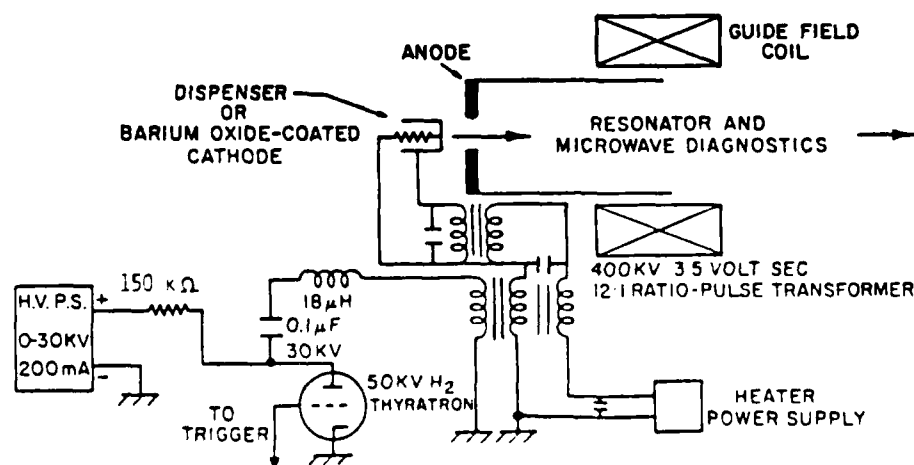


FIG. 6. A schematic diagram of the electron beam generator for the Čerenkov microwave experiments.

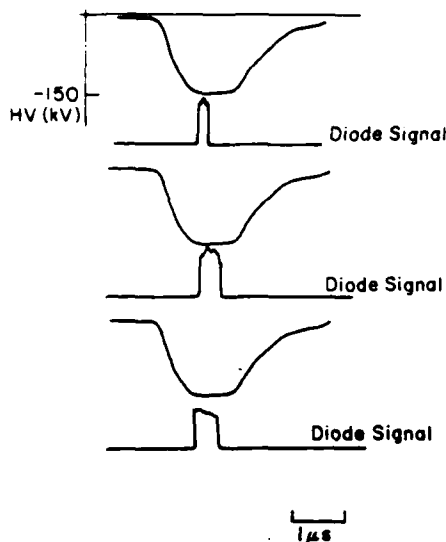


FIG. 7. Oscilloscope traces of the accelerating voltage and the resultant Čerenkov microwave pulse. Data taken past an 88-GHz high-pass filter.

until it is deposited on the waveguide walls. The beam current is monitored by observing the voltage across a $1-\Omega$ resistor to ground.

The microwave radiation produced is guided from the interaction region through a vacuum window and into a variety of diagnostic instruments. Power measurements are made using crystal detectors and calibrated pieces of attenuating material¹. The output frequency measurements are made using a diffraction grating spectrometer, a Fabry-Pérot interferometer, and high-pass filters.

A typical pulse sequence is shown in Fig. 7. The microwave output pulse width approaches the voltage pulse width

of the beam generator. In this sequence, boron-nitride-lined waveguides are used and threshold currents of as low as 1.5 A are obtained. This agrees well with the predicted threshold currents. The rise and fall times of the pulse are very fast, and this is consistent with the predicted growth rates, which are in the range of $4-9 \times 10^9 \text{ sec}^{-1}$ for these experimental results.

The frequency tunability of the Čerenkov maser is clearly demonstrated in Fig. 8. A theoretical plot of the synchronous frequency for the TM_{01} mode is included for comparison. The systematic displacement of the data to higher frequencies at lower energies may result from charging of the dielectric liner. It is possible that the 1/2-mm-thick liners used in these experiments intercepted some beam current, resulting in a bias. Biasing the beam to lower voltages would result in a higher synchronous frequency.

Microwave radiation in excess of 300 GHz has also been observed. These frequencies were determined with a series of high-pass filters. At these higher frequencies, the estimated power level at the diode junction is only a few watts, but the losses in the output guide are much higher at the shorter wavelengths. The transverse liner dimensions and accelerating voltage give very good agreement with the observed frequency if operation on the TM_{02} mode of the waveguide is assumed. Typical high-frequency pulses are usually very similar to the ones shown in Fig. 8. Occasionally, however, they show a very regular spiking which may be a result of natural mode locking of the very closely spaced axial modes.

Presented in Figs. 9 through 11 are the measured output power for the Čerenkov maser at operating frequencies of 80, 88, and 98 GHz, respectively. All the power measurements are taken with high-pass filters in the waveguide, allowing an estimate of the minimum operating frequency.

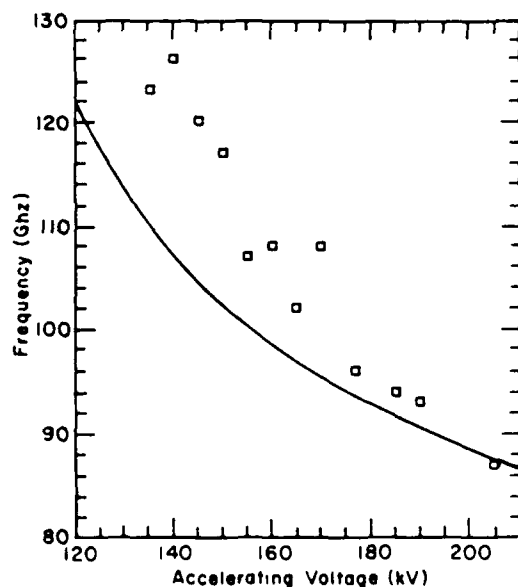


FIG. 8. Plot of the output microwave frequency, obtained using the diffraction grating spectrometer, as a function of beam voltage. The theoretical plot of the synchronous frequency for the TM_{01} mode is shown for comparison. The liner is 1/2 mm thick with an inner radius of 0.195 cm.

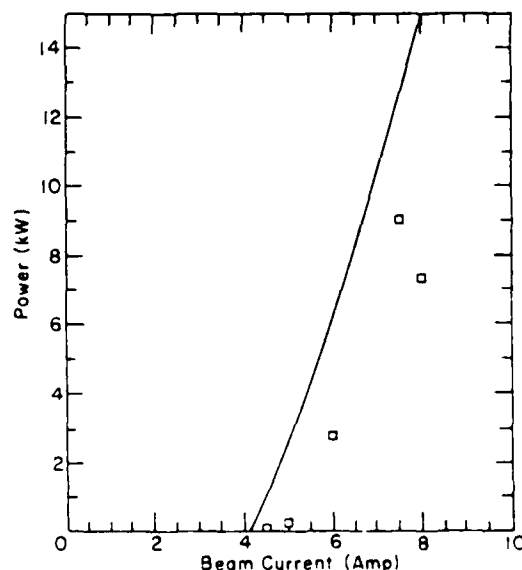


FIG. 9. Power output as a function of beam current for a fixed accelerating voltage of 150 kV. The theoretically predicted power is shown for comparison (see text). The liner is 1/2 mm thick with an inner radius of 0.25 cm. All data was taken past a 98-GHz filter.

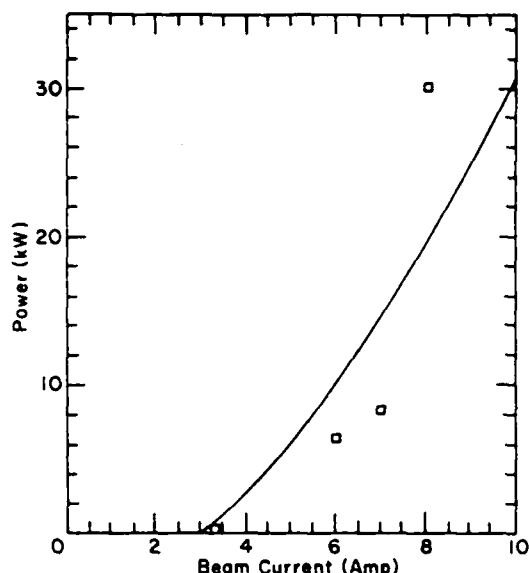


FIG. 10. Power output as a function of beam current for a fixed accelerating voltage of 155 kV. The liner geometry is that of Fig. 2. All data was taken past an 88-GHz filter.

The observed frequencies agree well with those predicted theoretically for operation on the TM_{01} mode of the waveguide at the accelerating voltages indicated.

The power measurements are made using calibrated pieces of microwave-absorbing material (eccosorb) and a $1N53$ diode in a Ka band mount. The system is calibrated using 65- and 85-GHz Gunn diodes and a 60-90-GHz sweep oscillator. The power output of the Gunn diodes and sweep oscillator is measured using a thermister mount, which is calibrated for 60-90 GHz. The $1N53$ diode response, terminated into $50\ \Omega$, is measured on an oscilloscope. A sensitivity of 2 mV/mW is a conservative estimate of the diode response for the 60-90-GHz frequency region.

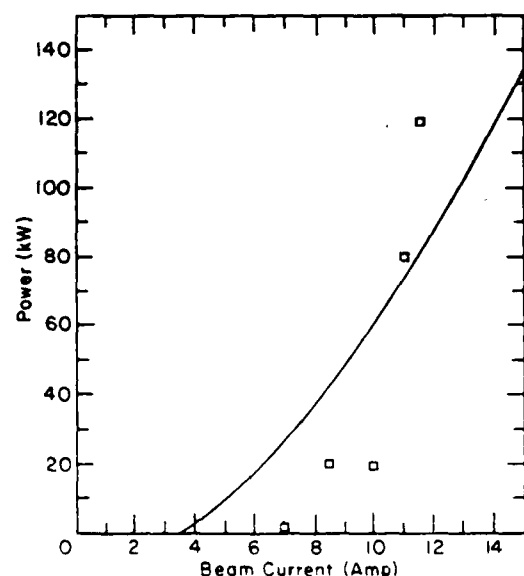


FIG. 11. Same as Fig. 10. Here, the accelerating voltage is 180 kV. All data was taken past an 80-GHz filter.

The solid line in Figs. 9, 10, and 11 represents theoretically predicted power output for the Čerenkov maser. The calculation is based on the assumption that the axial component of the electric field grows until it reaches a level which is sufficient to trap electrons and then ceases to grow further. The assumption thus yields an estimate for the electric field, which is a function of the beam parameters and the dispersion relation. This is, in turn, used to calculate the stored energy and the output power. The reflectivity of the cavity and the beam-dielectric gap are adjusted to fit the observed threshold currents for each dielectric liner used. Very little power is detected until the threshold current is reached and above threshold output power increases very rapidly with beam current. In this operating regime the saturating power will depend on $I^{4/3}$, where I is the total beam current. Typical operating efficiencies are between 1-5% in the 3-4-mm wavelength region, and efficiencies of 10% at 1 cm have been attained.

IV. TWO-STAGE DEVICES

A slow-wave resonant structure, consisting of a periodic arrangement of washers, was used to generate power for testing the diagnostics employed in the experiments. Washer spacing was 1/2 cm, and the ratio of inner to outer diameter of the washer was 1/2. The slow wave structure alone produced output pulses between 1 and 2 μ s in duration with power levels up to 1 kW. Fundamental output frequency was 30 GHz, but the output radiation was very rich in harmonic structure and power levels of 10 W at 100 GHz were easily detected.

The output power of 1 kW indicated strong bunching of the electron beam at the radiation wavelengths. This, in turn, suggested the possibility of using the periodic slow-wave structure as a prebuncher for the electron beam and a dielectric-loaded waveguide as an amplifier. The transverse dimensions of the dielectric liner were chosen to give a synchronous frequency of 30 GHz at 150 kV accelerating voltage. A schematic diagram of such a two-stage device is shown in Fig. 12.

The main results of the series of experiments performed using two-stage devices are shown in Figs. 13(a)-13(c). The output pulse width of the single-stage Čerenkov maser using this relatively thick (1.5 mm) liners is much narrower than the peak voltage pulse width. However, the two-stage resonator always resulted in broader output pulses. The power output of the two-stage device was at least as great and frequently 15 dB greater than the power output of the single-

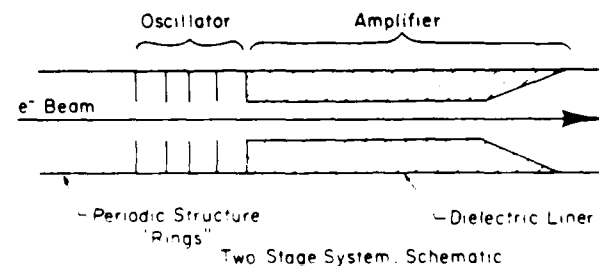


FIG. 12. Schematic diagram of the two-stage resonant device

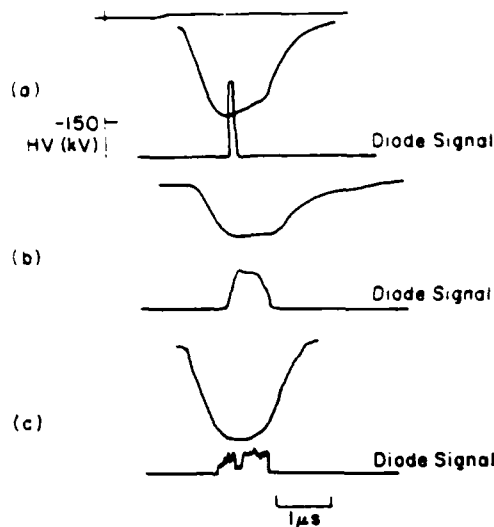


FIG. 13. (a) Oscilloscope traces of the accelerating voltage and resultant Čerenkov radiation for a 1.5-mm-thick dielectric liner. (b) Oscilloscope traces of the accelerating voltage and microwave output for the periodic slow-wave structure. (c) Resultant radiation for the combined slow-wave structure and dielectric liner.

stage, dielectrically lined guide. Up to 50 kW was detected at 30 GHz. It is very likely that amplification at the fundamental frequency was observed.

V. CONCLUDING REMARKS

In summary, Čerenkov masers can be potentially useful devices for generating high-power, tunable microwaves.

Nonoptimized operating efficiencies of 1–10% and the capability of generating radiation at wavelengths less than the transverse dimensions of the guide indicate the potential of the device as a source of lower- and submillimeter radiation.

Two-stage devices could be scaled down in transverse dimensions so that the output frequencies are in the lower-mm wavelength region. Although no attempt was made to optimize the two-stage devices, it should be possible to obtain higher operating efficiencies using a two-stage resonator.⁶

ACKNOWLEDGMENTS

This work was supported in part by U. S. Army Research Office Contract DAAG29-83-K-0018 and Air Force Office of Scientific Research Contract 82-0168. Also acknowledged is the assistance of Bernadette Johnson of Dartmouth College Plasma Laboratory.

¹K. L. Felch, K. O. Busby, R. W. Layman, D. Kapilow, and J. E. Walsh, *Appl. Phys. Lett.* **38**, (8), 601 (1981).

²S. Von Laven, J. Brancum, J. Golub, R. Layman, and J. Walsh, *Appl. Phys. Lett.* **41**, (5), 408 (1982).

³*Stimulated Čerenkov Radiation*, J. Walsh, *Proc. of the School on Physics of Quantum Electronics*, ed. S. Jacobs, Vol. 5 (Addison-Wesley, Reading, MA, 1978).

⁴*Čerenkov and Čerenkov Raman Radiation Sources*, J. Walsh, in *Physics of Quantum Electronics*, ed. S. Jacobs, Vol. 7 (Addison-Wesley, Reading, MA, 1980).

⁵M. Abele, *Nuovo Cimento* **9**, 207 (1952).

⁶P. Coleman and C. Enderby, *J. Appl. Phys.* **31**, 1695 (1960).

⁷J. Walsh and J. Murphy, *IEEE J. Quantum Electron.* **QE-18**, 1259 (1982).

⁸*Čerenkov Lasers in the Compton Regime*, J. Walsh and B. Johnson, *Proc. of the 4th Int. Conf. on Free Electron Lasers*, #453-26, Orcas Island, WA, June 1983.

The Cerenkov Maser at Millimeter Wavelengths

E. P. GARATE AND JOHN E. WALSH

Abstract—The dispersion relation for the transverse magnetic modes (TM_{0n}) of a partially filled, dielectric-lined, cylindrical waveguide driven by a cold relativistic electron beam is derived. The effect of a gap between the electron beam and the dielectric liner is included. The dispersion relation is then used to calculate the growth rate for the Cerenkov instability in the collective tenuous beam limit. Expressions are developed for the minimum current necessary for oscillation threshold and for the power output of the Cerenkov maser in the collective regime.

I. INTRODUCTION

THE COUPLING of a slow-guided electromagnetic wave and the slow space-charge mode of an electron beam can be a source of coherent, tunable, high-power, millimeter-wavelength radiation. If a dielectric-lined waveguide is used as the resonant slow-wave structure and it is driven by a relativistic electron beam, the resulting Cerenkov instability can bunch the electron beam and generate microwave radiation.

Spontaneous Cerenkov radiation is emitted as the electron beam traverses the dielectric-lined waveguide. Threshold for the emission occurs when the electron velocity v is greater than the speed of light in the dielectric $c/\sqrt{\epsilon}$ (c is the speed of light in vacuum and ϵ is the dielectric constant). The emitted radiation modulates the electron beam which does further work on the radiation amplitude of one of the transverse magnetic (TM) modes of the waveguide (stimulated emission). The frequency is determined by the synchronism between the electron velocity and the phase velocity of the driven mode [1] (see also [2], which contains many references to early work). It is possible to couple into all TM modes of the waveguide, but the growth rate for successive higher-order modes will decrease.

In early experiments [3], several megawatts of coherent radiation at 60 GHz were produced using a 750-keV 2-kA electron beam and a dielectric-lined guide. More recently [4]–[6], the tunability, efficiency, and high-power capability of a Cerenkov maser in the millimeter-wavelength region has been demonstrated. Power levels of 120 kW at 80 GHz at approximately 4-percent efficiency were recorded [6]. Relatively modest repetition-rated accelerating voltages (125–200 kV) and beam currents (20 A) were employed in the latter experiments. However, the current density (100 A/cm²) was large, and thus it is

expected that the Cerenkov maser was operating in the collective regime for these experiments.

A theoretical description of the Cerenkov maser in the single-particle regime can be found in [7]. It is the goal of the present work to present a similar theoretical description of the Cerenkov maser in the collective regime. The slow waveguide modes evanesce away from the dielectric liner, and a beam-dielectric gap will degrade coupling. Consequently, the effect of such a gap is included in the theoretical description. Furthermore, the choice of cylindrical geometry is used throughout so that a comparison can be made between theory and the experimental results of [6].

The organization of the remainder of this work is as follows. In Section II, the linearized fluid and Maxwell's equations and the cold-beam approximation are used to derive the dispersion relation for the TM_{0n} modes of the coupled electron-beam gap dielectric-lined waveguide. Included is a discussion of the no-beam dispersion relation and the expected scaling of the output frequency with dielectric-lined dimensions. In Section III, the complete dispersion relation is used to derive the growth rate for the Cerenkov interaction in the tenuous beam limit. Expressions for the oscillation threshold currents and power output for the Cerenkov maser are presented in Sections IV and V, respectively. A conclusion section follows.

II. DISPERSION RELATION

The solutions of the linearized fluid and Maxwell's equations for the electric field \bar{E} and the magnetic field \bar{B} are found for a cylindrical waveguide geometry which includes a cold electron beam contained by an infinite axial magnetic guide field. The assumption of an infinite magnetic guide field constrains the electron motion to the axial direction, which is chosen to be the z axis. In practice, a field of 2–3 kG will ensure the accuracy of this approximation [8]. Application of the appropriate boundary conditions of the displacement vector \bar{D} and the electric field \bar{E} leads to the dispersion relation for the electron-beam dielectric-lined waveguide system. The only modes considered in the analysis are azimuthally symmetric modes which can axially bunch the electron beam, i.e., TM_{0n} modes.

Assuming a plane-wave dependence on axial position z and time t , the fields, velocities, charge, and current densities can be written as

$$\bar{E} = (E_r(r) \hat{r} + E_z(r) \hat{z}) e^{ik_z z - i\omega t}$$

$$\bar{B} = B_\theta(r) e^{ik_z z - i\omega t}$$

Manuscript received April 1, 1985; revised July 3, 1985. This work was supported in part by AFOSR Grant 82 0168 and in part by ARO Grant DAAG 29 83 K 0018.

The authors are with the Department of Physics and Astronomy, Dartmouth College, Hanover, NH 03755.

$$\begin{aligned}\bar{v} &= v_0 \hat{z} + v_1(r) \hat{z} e^{ikz - i\omega t} \\ n &= n_0 + n_1(r) e^{ikz - i\omega t} \\ \bar{J} &= J_0 + J_1 = -n_0 e v_0 \hat{z} - e[n_0 v_1(r) + n_1(r) v_0] \hat{z} e^{ikz - i\omega t}\end{aligned}\quad (1)$$

where \hat{r} , $\hat{\theta}$, \hat{z} are the usual unit vectors in cylindrical coordinates and the subscripted field quantities refer to field components in the coordinate system. Here $v_1(r)$ and $n_1(r)$ are small velocity and density perturbations away from the unperturbed velocity and density v_0 and n_0 , respectively. The magnitude of the electron charge is e , and k and ω denote the wavenumber and angular frequency of the mode, respectively.

Expressions for $n_1(r)$, $v_1(r)$, and $J_1(r)$ in terms of the z component of the electric field result from the continuity

$$\frac{\partial \rho}{\partial t} + \bar{\nabla} \cdot \bar{J} = 0 \quad (2a)$$

$$\rho = -ne \quad (2b)$$

and the Lorentz force equations

$$\frac{d}{dt} \left(\frac{m_0 \bar{v}}{(1 - v^2/c^2)^{1/2}} \right) = -eE_z \hat{z} \quad (3)$$

Linearizing and manipulating (2) and (3) yields the expressions

$$n_1(r) = \frac{-iken_0 E_z(r)}{m_0 \gamma_0^3 (kv_0 - \omega)^2} \quad (4a)$$

$$v_1(r) = \frac{-eE_z(r)}{im_0 \gamma_0^3 (kv_0 - \omega)} \quad (4b)$$

$$J_1(r) = \frac{in_0 e^2 \omega E_z(r)}{m_0 \gamma_0^3 (kv_0 - \omega)^2} \quad (4c)$$

where γ_0 is the usual relativistic factor, $\gamma_0 = (1 - v_0^2/c^2)^{-1/2}$, and m_0 is the electron rest mass.

Substituting these expressions into Maxwell's equations (neglecting the static fields)

$$\begin{aligned}\bar{\nabla} \cdot \bar{E} &= \frac{-4\pi n_1(r)e}{\epsilon} \\ \bar{\nabla} \cdot \bar{B} &= 0 \\ \bar{\nabla} \times \bar{E} &= -\frac{1}{c} \frac{\partial \bar{B}}{\partial t} \\ \bar{\nabla} \times \bar{B} &= \frac{4\pi}{c} \bar{J} + \frac{1}{c} \frac{\partial \bar{D}}{\partial t}\end{aligned}\quad (5)$$

and manipulating the two curl equations results in the following differential equation for $E_z(r)$:

$$\left\{ \frac{1}{r} \frac{\partial}{\partial r} \left(r \frac{\partial}{\partial r} \right) + \left(\frac{\omega^2 \epsilon}{c^2} - k^2 \right) \left(1 - \frac{\omega_p^2}{\epsilon \gamma_0^3 (\omega - kv_0)^2} \right) \right\} \times E_z(r) = 0 \quad (6)$$

where ω_p is the beam plasma frequency, given by $\omega_p^2 = 4\pi n_0 e^2 / m$. The relationship between $E_r(r)$ and $E_z(r)$ is also found from Maxwell's equations:

$$E_r(r) = \frac{ik}{(\omega^2 \epsilon / c^2 - k^2)} \frac{\partial E_z(r)}{\partial r} \quad (7)$$

This relationship is needed when applying boundary conditions to arrive at a dispersion relation.

In the beam and gap region $\epsilon = 1$ and for slow-wave solutions $\omega^2/c^2 - k^2 < 0$.

Recognizing that the differential equation is Bessel's equation, the solution for $E_z(r)$ inside ($r < r_b$) the beam, gap and dielectric regions become

$$\begin{aligned}E_z(r) &= AI_0(pTr) \quad (r < r_b) \\ E_z(r) &= BI_0(pr) \\ &\quad + CK_0(pr) \quad (r_b < r < a) \\ E_z(r) &= D[J_0(qr) Y_0(qb) \\ &\quad - Y_0(qr) J_0(qb)] \quad (a < r < b)\end{aligned}\quad (8)$$

where the electron beam radius is r_b and a , b are the inner and outer radii of the dielectric liner, respectively. The radial fields follow from the application of (7).

The expression T appearing within the argument of I_0 in the beam region is the beam (longitudinal) index of refraction:

$$T = \left(1 - \frac{\omega_p^2}{\gamma_0^3 (\omega - kv_0)^2} \right)^{1/2}$$

Also not identified are the wavenumbers in the dielectric, $q^2 \equiv \omega^2 \epsilon / c^2 - k^2$ and $p^2 \equiv k^2 - \omega^2 / c^2$, respectively.

The expressions $J_n(x)$ and $Y_n(x)$ are ordinary Bessel's functions of order n of the first and second kind, respectively; $I_n(x)$ and $K_n(x)$ are modified Bessel's functions of the first and second kind, respectively. Use has been made of the boundary condition at the metallic guide $E_z(r = b) = 0$ in writing (8).

Applying the boundary conditions of continuity for the longitudinal electric field and radial component of the displacement vector at the beam-vacuum and vacuum-dielectric interfaces yields the following dispersion relation [9] for the beam gap dielectric-waveguide system:

$$\begin{aligned}D(u, v, w, x, y) &= -\frac{T}{p} sn(u, v) SH(w, 0) CH(x, y) \\ &\quad + \frac{\epsilon}{q} cs(u, v) CH(w, 0) ch(x, y) \\ &\quad + \frac{sn(u, v)}{p} CH(w, 0) SH(x, y) \\ &\quad - \frac{\epsilon}{q} Tcs(u, v) SH(w, 0) sh(x, y) = 0\end{aligned}\quad (9)$$

where $u = qa$, $v = qb$, $x = pr_b$, $y = pa$, and $w = pTr_b$. The radial trigonometric and hyperbolic functions are defined as follows:

$$\begin{aligned} sn(u, v) &= \frac{\pi v}{2} [J_0(v) Y_0(u) - Y_0(v) J_0(u)] \\ cs(u, v) &= \frac{\pi v}{2} [Y_0(v) J_1(u) - J_0(v) Y_1(u)] \\ SH(x, y) &= y[I_1(y) K_1(x) - K_1(y) I_1(x)] \\ CH(x, y) &= y[I_1(y) K_0(x) - I_1(x) K_0(y)] \\ sh(x, y) &= y[I_0(y) K_0(x) - I_0(x) K_0(y)] \\ ch(x, y) &= y[K_0(y) I_0(x) + I_0(y) K_1(x)]. \end{aligned} \quad (10)$$

III. THE LIMIT OF ZERO BEAM DENSITY

The expression for the no-beam dielectric-lined waveguide dispersion results if $\omega_p^2 = 0$:

$$\begin{aligned} D &= \frac{1}{p} SH(y, 0) sn(u, v) \\ &- \frac{\epsilon}{q} CH(y, 0) cs(u, v) = 0. \end{aligned} \quad (11)$$

Also, in the limit of no-beam-dielectric gap, i.e., $r_b \rightarrow a$, the dispersion relation becomes

$$\begin{aligned} D &= \frac{T}{p} SH(j, 0) sn(u, v) \\ &+ \frac{\epsilon}{q} cs(u, v) CH(j, 0) = 0 \end{aligned} \quad (12)$$

where $j = pTa$.

Both of these expressions agree with those in [10] for the appropriate limit. The output radiation frequency is approximately the frequency for which electron beam and phase velocity are in synchronism $\omega = kv_0$, thus the solutions of the no-beam dispersion relation give the expected operating frequency of the Cerenkov maser for a given electron velocity (in the limit $\omega_p \ll \omega$).

Certain characteristics of a Cerenkov maser can be inferred from Figs. 1 to 3. Shown in Figs. 1 and 2 are typical dispersion and voltage tuning curves. The Cerenkov maser is voltage tunable. As the beam velocity increases from threshold, the point of synchronism moves down along the dispersion curve, lowering the operating frequency of the device. Also, for a fixed beam velocity, lowering the dielectric constant, decreasing the liner thickness, or decreasing the transverse dimensions of the waveguide results in a higher operating frequency. This occurs because the cutoff frequency of the waveguide is increased. In general, short-wavelength operation can be achieved by using small transverse dimensions for the waveguide and thin dielectric tubes of low permittivity as liners. The relation of axial electric field E_z and waveguide geometry is illustrated in Fig. 3.

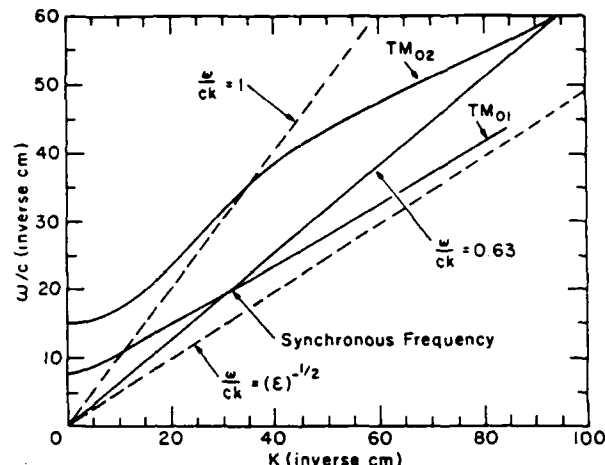


Fig. 1. Dispersion curve for a dielectric cylindrical waveguide. Shown are the TM_{01} and TM_{02} waveguide modes. The expected output frequency is given by the intersection between the beam dispersion (shown for $\omega/c k = 0.63$) and the waveguide dispersion curves.

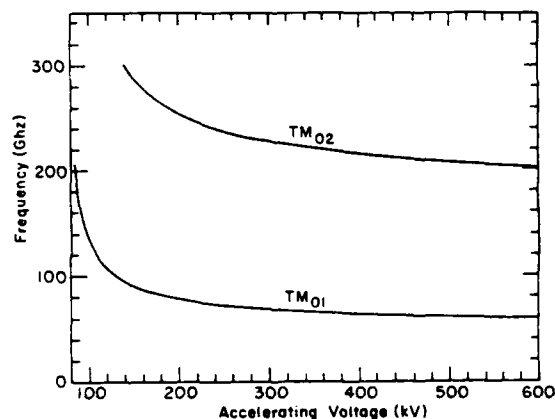


Fig. 2. Voltage tuning curves (11) for the first two TM modes of a cylindrical dielectric liner of 0.57 mm thickness. The inner radius is 0.241 cm and the dielectric is boron nitride ($\epsilon = 4.2$).

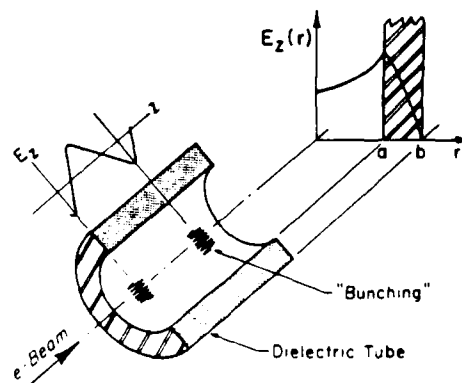


Fig. 3. The assumed configuration of a millimeter-wavelength cylindrical Cerenkov maser. The axial field component of the TM mode is evanescent in the beam channel region, and drops from a peak at the inner liner radius a to zero at the guide radius b .

The experiments of [4]–[6] indicate that the agreement between the theoretically predicted tuning curves for a large range of liner thicknesses and dielectric constant is

very good. This is the case for both the fundamental and harmonic modes of the waveguide.

III. LINEAR GROWTH RATE

Calculation of the growth rate in the collective regime proceeds from the dispersion relation for the lined waveguide-coupled system (9). Expanding the complete dispersion relation around the root of the empty waveguide dispersion function, and the electron susceptibility

$$4\pi\chi = \frac{\omega_p^2}{\gamma_0^3(\omega - kv_0)^2}$$

yields an algebraic equation for the complex frequency shift induced by the beam. The imaginary part of the shift determines the growth rate of the mode. Maximum growth occurs near synchronism ($\omega = kv_0 = \omega_{0k}$, where ω_{0k} is the solution of the dispersion relation of the empty guide).

The formal expansion of the dispersion relation takes the form

$$D(u, v, x, y) = D(\omega_{0k}, k_0) + (\omega - \omega_{0k}) \left. \frac{\partial D(u, v, \dots)}{\partial \omega} \right|_{\omega_{0k}} + \chi \left. \frac{\partial D}{\partial \chi} \right|_{\chi=0} + \dots$$

where $D(\omega_{0k}, k_0) = 0$ is the dispersion relation in the absence of the beam. Straightforward but lengthy manipulation of the no-beam dispersion relation for the dielectric-lined waveguide and identities involving the radial trigonometric functions results in the following expressions:

$$\left. \frac{\partial D}{\partial \omega} \right|_{\omega_{0k}} = \frac{\omega_{0k} SH(y, 0)}{c^2 \chi} L(u, v, y, \epsilon) \quad (13)$$

where

$$L(u, v, y, \epsilon) = \left[\frac{b^2 \epsilon}{aqpc s(u, v)} - sn(u, v) \left(\frac{2}{p} \left(\frac{1}{p^2} + \frac{\epsilon}{q^2} \right) + \frac{a CH(y, 0)}{SH(y, 0)} \left(\frac{1}{p^2} + \frac{\epsilon^2}{q^2} \right) \right) \right] \quad (14)$$

and

$$\left. \frac{\partial D}{\partial \chi} \right|_{\chi=0} = \frac{\omega_p^2 r_b}{2\gamma_0 a p} CH(y, 0) sn(u, v) \frac{\bar{n}}{n_0} \quad (15)$$

where \bar{n}/n_0 is defined by

$$\frac{\bar{n}}{n_0} = \frac{CH^2(x, 0) - SH^2(x, 0)}{CH^2(y, 0)} = \frac{\int_{\text{beam}} dA n |E_z|^2}{n_0 A_b |E_z|_{ref}^2} \quad (16)$$

The integral is over the cross-sectional area of the beam A_b and $(E_z)_{ref}$ is an axial reference value, here chosen at the dielectric-vacuum interface. The expression for effective density appears naturally in the solution.

After collecting terms, the expression for a cubic equation results:

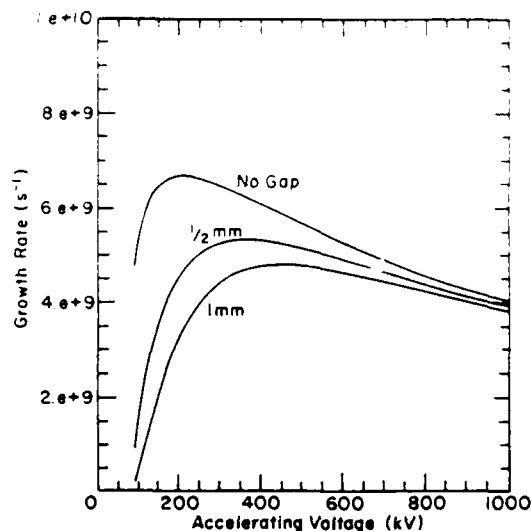


Fig. 4. The growth rate for the TM_{01} mode in the collective regime with beam-dielectric gap as the parameter. The electron density is adjusted to give 10-A beam current at 150 kV. The liner geometry is that of Fig. 2.

$$(\omega - kv_0)^2 (\omega - \omega_{0k}) = \frac{\omega_p^2}{\gamma_0^3} \frac{\partial D / \partial \chi}{\partial D / \partial \omega} = \frac{\omega_p^2 r_b^2 c^2 sn(u, v) CH(y, 0)}{2\gamma_0^3 \omega_{0k} a L(u, v, y, \epsilon) SH(y, 0)} \frac{\bar{n}}{n_0} \quad (17)$$

Invoking synchronism, the frequency shift and linear growth rate are:

$$\text{Re}(\omega - \omega_{0k}) = -\frac{1}{2} |\omega - \omega_{0k}|$$

and

$$\Delta \equiv \text{growth rate} = \frac{\sqrt{3}}{2} |\omega - \omega_{0k}|$$

where

$$|\omega - \omega_{0k}| = \frac{\sqrt{3}}{2} \left\{ \frac{\omega_p^2 r_b^2 c^2 sn(u, v) CH(y, 0)}{2\gamma_0^3 \omega_{0k} a L(u, v, y, \epsilon) SH(y, 0)} \frac{\bar{n}}{n_0} \right\}^{1/3} \quad (18)$$

The real part of the frequency shift is negative, which is expected since the beam velocity must be slightly larger than the phase velocity of the mode for the interaction to occur. Also, since the growth rate in the collective regime depends on ω_p^2 , the beam current dependence is $I^{1/3}$. This is to be compared to the linear dependence of the growth rate on beam current in the single-particle regime [7].

Referring to Fig. 4, note that the growth rate decreases exponentially near the threshold voltage and peaks at larger accelerating voltages for increasing beam-dielectric gaps. This results from the effective density \bar{n}/n_0 in the expression for the growth rate. Writing the effective density as

$$\frac{\bar{n}}{n_0} = \frac{CH^2(x, 0) - SH^2(x, 0)}{CH^2(y, 0)} = \frac{I_0^2(pr_b) - I_1^2(pr_b)}{I_0^2(pa)} \quad (19)$$

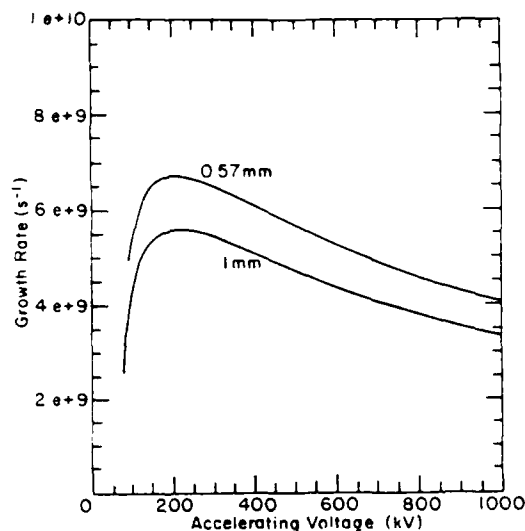


Fig. 5. The growth rate for the TM_{01} mode with liner thickness as the parameter. The inner radius of the liner is held constant at 0.241 cm. Beam density is that of Fig. 4, and there is no beam-dielectric gap.

and using $pr_b \gg 1$, then

$$\frac{\bar{n}}{n_0} \sim \exp \left[-\frac{2\pi d}{\lambda\beta\gamma} \right]$$

where $d = (a - r_b)$ is the beam-dielectric gap, and the assumption $\omega \approx k_0 v_0$ is employed. Since the operating wavelength λ approaches zero at the threshold voltage, the growth rate decreases exponentially. An increase in beam-dielectric gap requires an increase in $\lambda\beta\gamma$ to ensure good beam-mode coupling. The important result, $\lambda\beta\gamma \sim d$ for good coupling, has been previously derived for the single-particle limit [7]. Although not indicated in Fig. 4, the growth rate approaches zero for $\beta \rightarrow 1$. This occurs because the increase in the relativistic mass of the electrons makes bunching more difficult. This limit is not important in devices designed for millimeter-wavelength operation, but it becomes a factor in far-infrared Cerenkov laser design [11].

The above characteristics of the growth rate do not depend on the specific dimensions of the dielectric liner. However, the magnitude of the growth rate and the accelerating voltage at which the growth rate peaks do depend on the transverse dimensions. Fig. 5 shows the growth rate for two different liner dimensions. These are chosen to coincide with those used in [4]–[6]. It should be noted that the device with the thinner liner will operate at a higher frequency so long as the gap parameter ($2\pi d/\lambda\beta\gamma$) remains small (≤ 1).

IV. THE OSCILLATION THRESHOLD CURRENTS

The minimum current needed for oscillation threshold in the collective regime depends on the growth rate. In the present discussion, only the output coupling losses of the resonant cavity are taken into account. Absorption losses in the dielectric at millimeter wavelengths are assumed negligible.

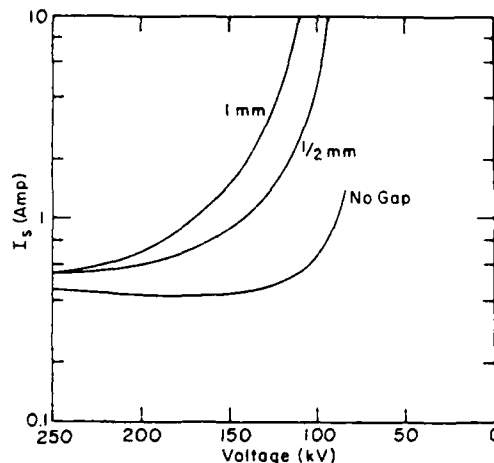


Fig. 6. The threshold currents necessary for oscillation in the collective limit with beam-dielectric gap as the parameter. The reflectivity is 50 percent and the liner geometry is that of Fig. 2.

The strength of the electron beam-waveguide mode interaction can be described in terms of a beam-quality factor Q_b defined by:

$$\frac{1}{Q_b} = \frac{1}{\omega\epsilon} \frac{\partial\mathcal{E}}{\partial t}$$

where \mathcal{E} is the energy stored in the radiation fields. Using $\partial\mathcal{E}/\partial t = 2\Delta\mathcal{E}$, this may be written as $1/Q_b = 2\Delta/\omega$. Oscillation occurs when the energy lost by the electron beam, per pass, is greater than the energy coupled out of the cavity. Expressing this in terms of the cavity quality factor Q_c , oscillation threshold occurs for

$$\frac{1}{Q_b} = \frac{2\Delta}{\omega} = \frac{1}{Q_c} \quad (20)$$

The output coupling Q of the cavity [12], neglecting attenuation losses, is

$$\frac{1}{Q_c} = \frac{\lambda}{4\pi L} \left(\frac{1 - R^2}{R^2} \right) \quad (21)$$

where R and L are the cavity reflectivity and length, respectively.

Combining (18), (20), and (21), the threshold current is given by the following expression:

$$I_s = \frac{1}{18\sqrt{3}} \left(\frac{\lambda}{4\pi L} \frac{[1 - R^2]}{R^2} \right)^3 \times \left(\frac{I_0 \beta \gamma_0^3 \omega^4 a SH(y, 0)}{pc^4 \bar{n}/n_0 sn(u, v) CH(y, 0)} \right) L(u, v, y, \epsilon) \quad (22)$$

where $I_0 = mc^3/e = 17$ kA.

The general features of this expression are exhibited in Fig. 6. The exponential increase in current needed to achieve oscillation near the Cerenkov threshold voltage and the rapid increase in the starting current for decreasing electron energy result from the decreasing growth rate, discussed in the previous section. Also, as expected, an

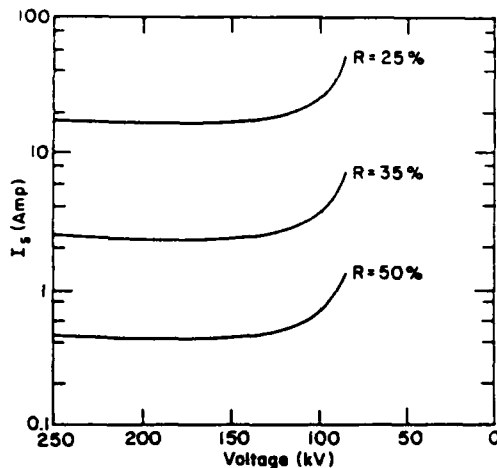


Fig. 7. The variation of threshold current with reflectivity. The parameters are the same as those of Figs. 2 and 6 and the beam-dielectric gap is zero.

increase in cavity reflectivity will decrease the beam current needed for oscillation. This is illustrated in Fig. 7.

Finally, it should be noted that the predicted threshold currents, shown in the above figures, agree well with the experimentally observed start currents in [6].

V. POWER OUTPUT

The time-averaged Poynting flux is used to calculate the power output of the Cerenkov maser in the collective regime. The power

$$P = \frac{c}{4\pi} \int_0^\tau \frac{dt}{\tau} \int [\text{Re}(\vec{E}) \times \text{Re}(\vec{B})] \cdot d\vec{A} \quad (23)$$

where $d\vec{A}$ is the cross-sectional area of the resonator and τ is the period of oscillation of the fields. Recognizing that only the radial part of the electric field $E_r(r)$ will contribute to the result and using Maxwell's equations to relate $B_\theta(r)$ to $E_r(r)$ yields

$$|B_\theta| = \left| \frac{\omega\epsilon}{ck} E_r(r) \right| \quad (24)$$

and the time-averaged power output becomes

$$P = \frac{k\omega}{4} |A|^2 \left\{ -\frac{a^2}{2} \left(\frac{1}{p^2} + \frac{\epsilon}{q^2} \right) - \frac{a^2}{2p^3} \left(\frac{1}{\epsilon} - 1 \right) \left[\frac{SH(y, 0)}{CH(y, 0)} \right]^2 - \frac{a}{p} \frac{SH(y, 0)}{CH(y, 0)} \left(\frac{1}{p^2} + \frac{1}{q^2} \right) + \frac{b^2\epsilon}{2q^2 sn^2(u, v)} \right\} \quad (25)$$

The boundary conditions on the displacement vector and (7) have been used to relate the radial field amplitude.

Using the following corrected orbit rate equation [13] for the longitudinal field amplitude A (an analytic approximation to trapping)

$$\frac{\partial A}{\partial t} - 2\Delta A + \frac{k^2\epsilon^2}{m_0^2\gamma^6\Delta^3} |A|^2 A + \frac{\omega}{Q_c} A = 0 \quad (26)$$

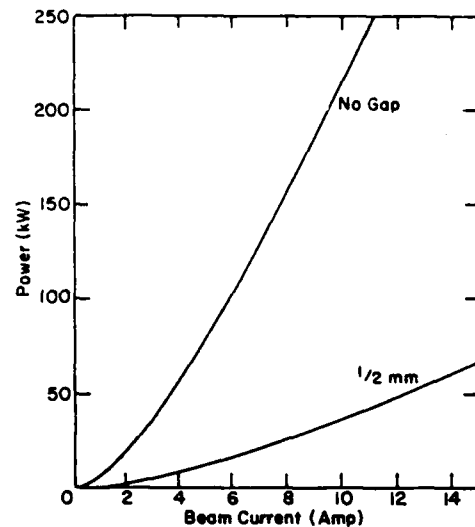


Fig. 8. The effect of the beam-dielectric gap on power output. The liner geometry is that of Fig. 2, the reflectivity is 50 percent, and the accelerating voltage is 180 kV. The output frequency is approximately 80 GHz (see tuning curve, Fig. 2).

it is possible to estimate the power output at saturation. Note that apart from the nonlinear term in the above equation, the rate of change of the axial field with time is due to the growth rate of the interaction Δ and the rate at which energy is coupled out of the cavity ω/Q_c .

At saturation, $\partial A/\partial t = 0$, therefore

$$A^2 = \frac{2m_0^2\Delta^4\gamma^6}{k^2\epsilon^2} \left(1 - \left(\frac{I_s}{I} \right)^{1/3} \right) \quad (27)$$

where $\omega/2\Delta Q_c = (I_s/I)^{1/3}$ has been used. Neglecting the cavity loss term $(I_s/I)^{1/3}$, this would be the expression, to within a factor of unity, that results from 100-percent bunching, i.e., $n_1 = n_0$ in (4a) ($\Delta = \sqrt{32} |kv_0 - \omega| \lambda$).

Because of the dependence of the saturated field on growth rate, the power output of the Cerenkov maser, for a fixed electron-beam energy and for beam currents much larger than the threshold current, will depend on the current to the fourth-thirds power $I^{4/3}$ (see (25)). Furthermore, because of the $I^{4/3}$ dependence, small beam-dielectric gaps can have a significant effect on the power output of the device. This is clearly demonstrated in Fig. 8. The operating efficiency for a device with liner dimensions of the previous figure is shown in Fig. 9. The increase of efficiency with beam current will ultimately be limited by debunching effects.

Adjustment of the cavity reflectivity and beam-dielectric gap can result in a very rapid rise in predicted power output near the threshold current (Fig. 10). The magnitude of the predicted power output and the rapid rise near threshold again agree well with the experimentally observed power output of [6]. It is also interesting to note that this elementary model-based estimate is in substantial agreement with a rigorous particle-code simulation [14].

VI. CONCLUSIONS

A theoretical description of the Cerenkov maser operating in the high-gain collective regime has been devel-

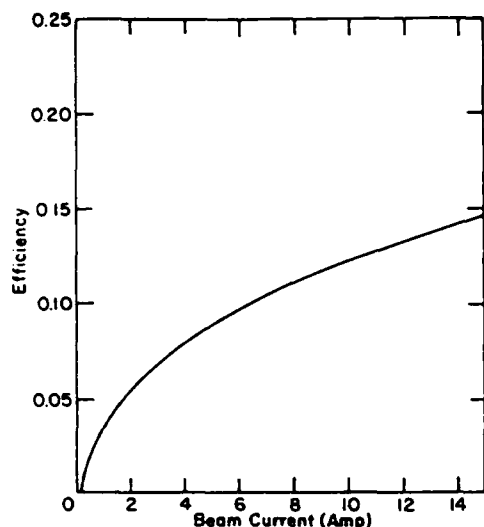


Fig. 9. Efficiency of a Cerenkov maser.

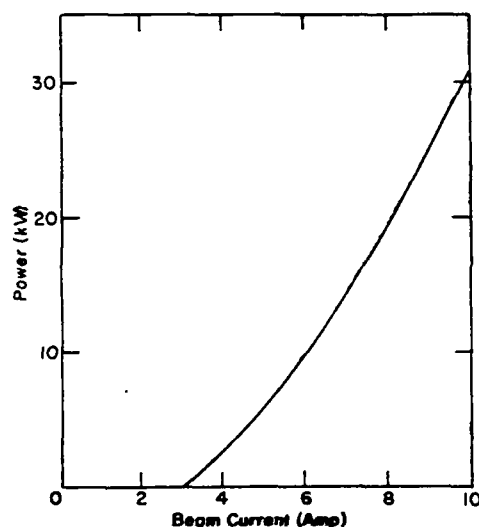


Fig. 10. The power output of the Cerenkov maser geometry in the preceding figures. The accelerating voltage is 155 kV, which corresponds to an output frequency of 88 GHz. The reflectivity is 37 percent and the beam-dielectric gap is 0.37 mm.

oped. The effect of the beam-dielectric gap on the growth rate, threshold current, and power output is shown to be important. However, if $\lambda\beta\gamma \sim d$ is maintained, then good coupling between the electron beam and waveguide modes is assured. This suggests the possibility of using relatively small transverse dimension liners and moderately relativistic beams ($\gamma \lesssim 2$) to generate tens of kilowatts of tunable, millimeter, or submillimeter microwave radiation.

The detailed results were developed under the assumption that the beam was not too dense. If the beam density

is increased arbitrarily, the tenuous beam approximation, i.e., $\chi \ll 1$, will not be applicable. In this case, a numerical solution to the complete dispersion relation presented in Section II will be necessary. Even if this limit is reached, the qualitative features of the interaction will remain the same.

Finally, it should be mentioned that in order to have better estimates of the saturated field amplitude, a complete nonlinear theory of the Cerenkov instability must be presented. This work is in progress. In spite of the qualitative nature of the nonlinear theory, the agreement with experimental observation is satisfactory.

ACKNOWLEDGMENT

The authors would like to acknowledge the substantial contributions made to the early phase of this work by Dr. K. Felch and Dr. S. Von Laven, as well as discussions held with B. Johnson on the relation between millimeter and far-infrared Cerenkov sources.

REFERENCES

- [1] M. Abele, "The Cerenkov effect in optics and in the microwave region," *Nuovo Cimento*, vol. 9, suppl. 3, pp. 207-213, 1952.
- [2] J. Walsh, "Cerenkov and Cerenkov-Raman radiation sources," in *Free Electron Generators of Coherent Radiation (Physics of Quantum Electronics)*, S. Jacobs, H. Pilloff, M. Sargent, M. Scully, and R. Spitzer, Eds. Reading, MA: Addison-Wesley, 1978, pp. 255-300.
- [3] J. E. Walsh, T. C. Marshall, and S. P. Schlesinger, "Generation of coherent Cerenkov radiation with an intense relativistic electron beam," *Phys. Fluids*, vol. 20, pp. 709-710, 1977.
- [4] K. L. Felch, K. O. Busby, R. W. Layman, D. Kapilow, and J. E. Walsh, "Cerenkov radiation in dielectric-lined waveguides," *Appl. Phys. Lett.*, vol. 38, pp. 601-603, 1981.
- [5] S. Von Laven, J. Branscum, J. Golub, R. Layman, and J. Walsh, "High-power Cerenkov maser oscillator," *Appl. Phys. Lett.*, vol. 41, no. 5, pp. 408-410, 1982.
- [6] E. P. Garate, R. Cook, P. Heim, R. Layman, and J. Walsh, "Cerenkov maser operation at lower-mm wavelengths," *J. Appl. Phys.*, vol. 58, no. 2, pp. 627-632, 1985.
- [7] J. E. Walsh and J. B. Murphy, "Tunable Cerenkov lasers," *IEEE J. Quantum Electron.*, vol. QE-18, no. 8, pp. 1259-1263, 1982.
- [8] W. B. Case, R. D. Kaplan, J. E. Golub, and J. E. Walsh, "Space-charge-Cerenkov and cyclotron-Cerenkov instabilities in an electron-beam dielectric system," *J. Appl. Phys.*, vol. 55, no. 7, pp. 2651-2658, 1984.
- [9] E. P. Garate, "Cerenkov masers at lower-millimeter wavelengths," Ph.D. dissertation, Plasma Lab., Dep. Physics & Astronomy, Dartmouth College, Hanover, NH, June 1985.
- [10] K. Felch, "Cerenkov Radiation in dielectric loaded waveguides," Ph.D. dissertation, Plasma Lab., Dep. Physics & Astronomy, Dartmouth College, Hanover, NH, Jan. 1980.
- [11] J. E. Walsh, B. Johnson, G. Dattoli, and A. Renieri, "Undulator and Cerenkov free-electron lasers: A preliminary comparison," *Phys. Rev. Lett.*, vol. 53, no. 8, pp. 779-782, 1984.
- [12] A. Yariv, *Introduction to Optical Electronics*. New York: Holt, Rinehart, and Winston, 1976, p. 114.
- [13] J. E. Walsh and J. S. Hagelin, "Van der Pol's equation and nonlinear oscillations in a beam plasma system," *Phys. Fluids*, vol. 19, no. 2, pp. 339-340, 1976.
- [14] A. T. Lin, W. W. Chang, and Y. T. Yan, "dc electric-field enhancement of Cerenkov-radiation output power," *IEEE Trans. Plasma Sci.*, vol. PS-13, no. 6, pp. 531-537, Dec. 1985.

Cerenkov maser operation at 1–2 mm wavelengths

E. P. Garate, S. Moustazis, J. M. Buzzi, C. Rouille, and H. Lamain
Laboratoire de Physique des Milieux Ionises, Ecole Polytechnique, Palaiseau Cedex, France

J. Walsh and B. Johnson
Department of Physics and Astronomy, Dartmouth College, Hanover, New Hampshire

(Received 10 September 1985; accepted for publication 25 March 1986)

The interaction of a dense ($n \sim 10^{12} \text{ cm}^{-3}$), mildly relativistic ($1.8 < \gamma < 3$) electron beam and a cylindrical, dielectric lined waveguide has produced tunable microwave radiation in the 150–310 GHz frequency range with an estimated power output of 500 kW at 150 GHz and 10 kW at 310 GHz. The measured output frequency agrees well with the frequency for which the phase velocity of the $\text{TM}_{0,1}$ mode of the dielectric lined guide is synchronous with the electron beam velocity.

Previous experimental results^{1–3} on the generation of stimulated Cerenkov radiation have demonstrated the wide tunability and high power capability of Cerenkov masers at centimeter and lower millimeter wavelengths. The cited works have also verified the dependence of output frequency on the transverse dimensions of the dielectric liner and demonstrated agreement between the theoretically predicted and the observed beam threshold parameters for threshold oscillation. In the work reported here, experimental results are presented which further verify the output frequency dependence on the transverse dimensions of the dielectric liner and display the wide tunability and high power capability of the Cerenkov maser in the 1–2 mm wavelength region.

Cerenkov radiation is produced when a charged particle traveling at superluminal velocities passes through or near a dielectric medium. If a resonant slow wave structure, such as a dielectric lined waveguide, is driven by a relativistic electron beam, the Cerenkov instability causes bunching of the electron beam by the axial electric field component of a $\text{TM}_{0,n}$ mode of the waveguide. For an electron beam that is strongly coupled to the radiation field, the growth rate for the Cerenkov instability can be sufficient to overcome the various loss mechanisms and stimulated emission occurs.

The frequency of the radiation emitted is determined by the beam velocity, the transverse dimensions of the dielectric liner, and the dielectric constant ϵ of the liner material. In general, the emitted radiation frequency increases for decreasing dielectric liner thickness and/or decreasing dielectric constant. For fixed dielectric liner dimensions lowering the electron beam accelerating voltage increases the frequency of the emitted radiation. Also, because the axial electric field evanesces into the beam region, any beam-dielectric gap will degrade coupling. However, good coupling can be maintained if $\text{gap}/\lambda\beta\gamma \sim 1$ (Ref. 4), where λ is the radiation wavelength, β is the electron beam velocity divided by the speed of light in a vacuum, and γ is the usual relativistic factor.

Since the minimum beam velocity needed for the interaction to occur is given by $\beta^2 = 1/\epsilon$ and because low dielectric constants result in higher output frequencies, relatively large accelerating voltages ($> 200 \text{ kV}$ for $\epsilon = 2$) are needed for operation in the 1–2 mm wavelength range. The advantage of relatively large accelerating voltages is that good coupling between the electron beam and the driven waveguide mode results. A discussion of the theory of devices based on stimulated Cerenkov radiation and a more detailed discus-

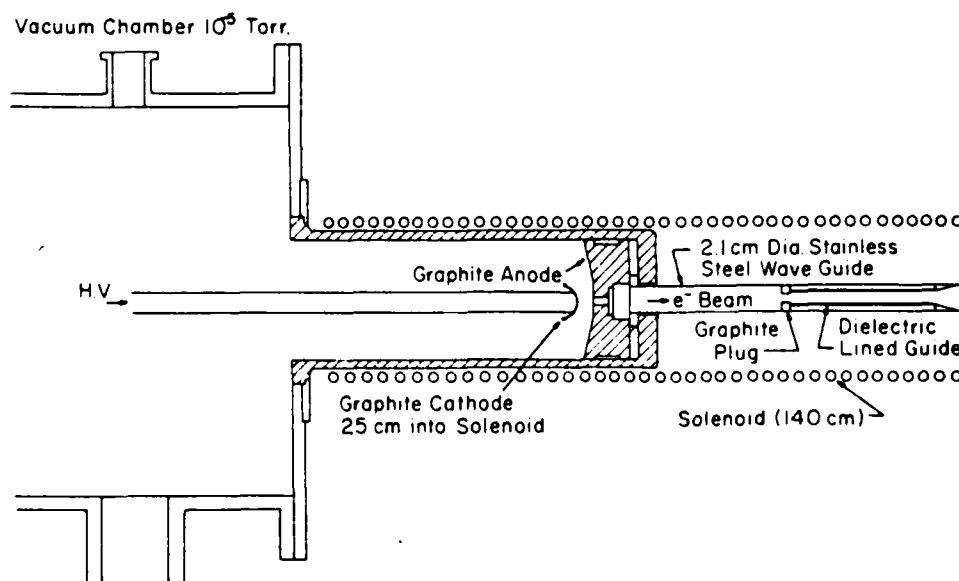


FIG. 1. Diode configuration and experimental geometry.

sion of the theory of cylindrical, dielectric lined, relativistic electron beam driven waveguides has been presented previously.^{4,6}

In this work, the electron beam is generated by a Physics International 110A capable of producing accelerating voltages between 400 kV and 1.5 MV with a pulse duration of 20 ns. Figure 1 shows the diode configuration, experimental geometry, and the solenoid which is used to confine and guide the electron beam into the resonant interaction region. The cathode is hemispherical with a radius of curvature of 3 cm and is separated from the concave anode, which has a 6-mm-diam aperture, by 8–10 mm. Both the anode and cathode are made of graphite. The cathode is placed 25 cm into the solenoid which is capable of generating a continuously variable, pulsed magnetic guide field up to 13 kG. This diode geometry can produce 1.4 kA of guide current at 1.2 MV.

The cylindrical dielectric lined waveguide is positioned 25 cm downstream from the anode and is centered inside a larger stainless-steel guide. The smaller waveguide is electrically connected to the larger guide which serves as the beam return to ground. Because the inner radius of the dielectric liners used was between 1 and 2 mm, a graphite plug was placed immediately before the dielectric lined waveguide to collimate the electron beam.

The microwave radiation produced is guided from the interaction region through a lens-shaped Teflon vacuum window into free space. A diffraction grating spectrometer, calibrated to operate in the 50–350 GHz frequency range, is placed a distance of up to 2 m away from the vacuum window. A pulse sequence from the grating spectrometer output

is shown in Fig. 2. Occasionally, the output pulse width approaches the voltage pulse width of the beam generator.

Figures 3 and 4 show the results of the measurement of frequency emission, using the grating spectrometer, as a function of the electron accelerating voltage. Independent verification of a minimum operating frequency was obtained by using high-pass filters with cutoffs of 100, 150, and 300 GHz. The solid line in the figures is the theoretical plot of the frequency for which the TM_{11} mode phase velocity is synchronous with the electron beam velocity. The output frequency is voltage tunable over a very wide range and the measured frequency agrees very well with the theoretically calculated output frequency.

In the results of Refs. 1–3 there is a systematic displacement of the data to frequencies higher than those predicted by the theory which does not appear in the present work. This is most likely due to interception of some of the beam current by the dielectric liner resulting in a bias voltage. Biasing the beam to lower voltages would result in higher synchronous frequencies. Because of the modest accelerating voltages (100–200 kV) used in the previous experiments even a small bias voltage of 10 kV would appreciably affect the output frequency. The dielectric liners used in the above experiments could support at least 20 kV bias voltage before dielectric breakdown occurred.

A measurement of the power output of the Cerenkov maser in the 150–200 GHz (Fig. 4) frequency range was made by placing a 4-mm detector horn a distance of 6 m away from the vacuum window. Referring to Fig. 5, several checks were made to be sure that the signal detected by the 1N53 diode used to estimate the power output was not due to reflection or noise produced by the voltage generator. For example, if the mirror was rotated, no signal was detected by the primary detection diode but a signal was detected by the secondary diode. Also, placing a piece of aluminum foil over the vacuum window resulted in no signal at either of the detection diodes. The estimate of the power output is made by calculating the power incident on the detector based on the power response of the 1N53 diode in an 8-mm wide band mount and by calculating the solid angle subtended by the 4-

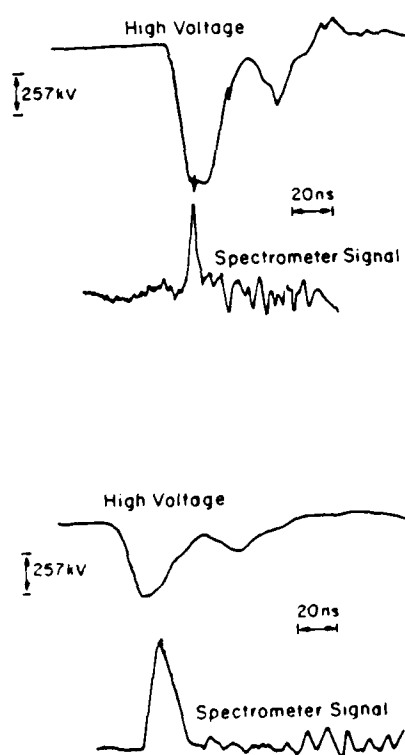


FIG. 2. Oscilloscope traces of the electron beam accelerating voltage and the resultant spectrometer output

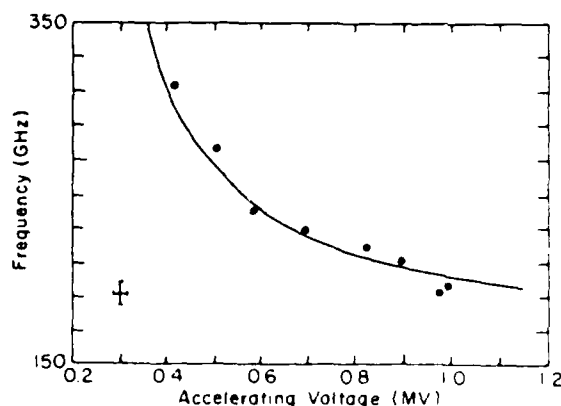


FIG. 3. Plot of the output microwave frequency as a function of the electron beam accelerating voltage. The theoretical plot of the synchronous frequency for the TM_{11} mode of the dielectric lined waveguide is shown for comparison. The dielectric liner is 1.4 mm thick with an inner radius of 1 mm. The liner is made of Teflon and is 35 cm long. The estimated error bars appear in the lower left-hand corner.

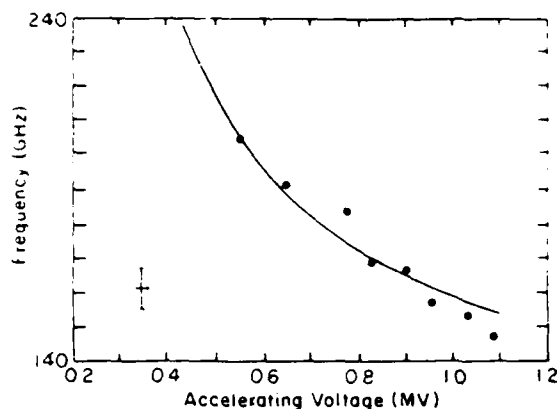


FIG. 4. Same as Fig. 3. Here, the liner is 1/4 mm thick with an inner radius of 1.75 mm. The liner is made of polyethylene and is 50 cm long.

mm horn. Using this method, the power output of the Cerenkov maser was 500 kW at 150 GHz and 40 kW at 200 GHz. All these measurements were taken past a 100-GHz high pass filter. Calculations of the growth rate for the Cerenkov maser of Fig. 4 operating in the collective, tenuous beam limit⁴ indicate that the power has undergone between 6 and 8 e foldings during the beam transit down the resonator. Even modest amounts of reflectivity at the ends of the dielectric liner could lead to the large power outputs measured.

After the power measurements were made, the current through the dielectric tube was measured using a 50-m Ω Faraday cup. At an accelerating voltage of 1 MV ($f \sim 150$ GHz) the current measured was 150 A and at 550 kV ($f \sim 200$ GHz) the current measured was 60 A. This yields efficiencies of 0.33% and 0.12% for microwave production at 150 and 200 GHz, respectively.

The estimate of the power output for the Cerenkov maser of Fig. 3 is 10 kW at 310 GHz. This is based on the detection threshold of the spectrometer used to measure the frequency of the microwave emissions. The signal detected by the spectrometer was at least a factor of 2 greater than the noise, so this represents a conservative estimate of the power output. The current measured through the dielectric liner of Fig. 3 at an accelerating voltage of 410 kV ($f \sim 310$ GHz) was 20 A, yielding an efficiency of 0.12%.

In conclusion, Cerenkov masers can be useful devices for generating tunable, high-power millimeter and submilli-

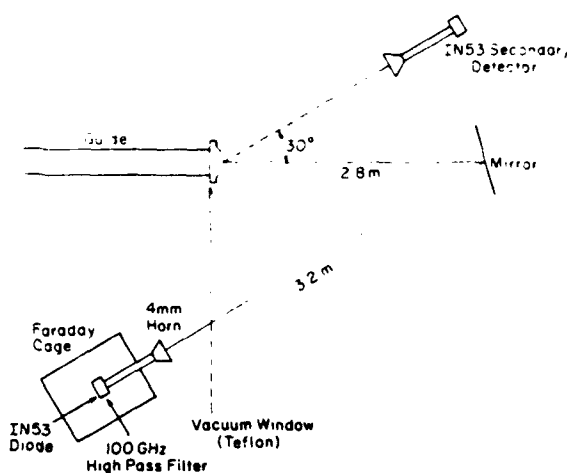


FIG. 5. Schematic diagram of the method used to measure the power output of the Cerenkov maser of Fig. 4.

meter wavelength radiation. Although the efficiencies for microwave production of the devices reported here are low, they are not unreasonable for an unoptimized super-radiant amplifier. Also, based on the data from the Cerenkov maser of Fig. 3, the quality of the beam generated in these experiments is high enough to be used as a beam source for a Cerenkov maser with 500 μ m wavelength radiation produced at 1–1.2 MV accelerating voltages. An experiment of this kind is currently being pursued.

This work was supported in part by Direction de Recherche Expérimentale et Théorique Contract 83-515/85-009, U.S. Army Research Office contract DAAG29-85-K-0176, and Air Force Office of Scientific Research contract 82-0168.

¹K. L. Felch, K. O. Busby, R. W. Layman, D. Kapilow, and J. E. Walsh, *Appl. Phys. Lett.* **38**, 601 (1981).

²S. Von Laven, J. Branscum, J. Golub, R. Layman, and J. Walsh, *Appl. Phys. Lett.* **41**, 408 (1982).

³E. Garate, R. Cook, P. Heim, R. Layman, and J. Walsh, *J. Appl. Phys.* **58**, 627 (1985).

⁴E. P. Garate and J. Walsh, *IEEE Trans. Plasma Science* **PS-13**, 524 (1985).

⁵J. Walsh, in *Physics of Quantum Electronics*, edited by S. Jacobs (Addison Wesley, Reading, MA, 1980), Vol. 7, pp. 255–300.

⁶J. Walsh, in *Advances in Electronics and Electron Physics* (Academic, New York, 1982), Vol. 58, pp. 271–310.

CERENKOV LASERS*

J. Walsh, B. Johnson, E. Garate, R. Cook, J. Murphy and P. Heim

Department of Physics and Astronomy, Dartmouth College, Hanover, N.H. 03755, U.S.A.

Abstract.-

A Cerenkov laser consists of an electron beam, a dielectric resonator, and suitable output coupling optics¹. The beam may pass directly through the dielectric at greater-than-light speed for that medium, in which case it will emit spontaneous Cerenkov radiation. If, in addition, there are mirrors forming an optical cavity, the reflected radiation stimulates further Cerenkov emission, and gain can result. In order to achieve gain, however, the beam velocity spread must be kept very low and hence in this most elementary case a gaseous dielectric and a highly energetic beam is needed. The Cerenkov threshold energy γ_T expressed in terms of the index of refraction n is given by:

$$\gamma_T = n / \sqrt{n^2 - 1}$$

When typical gasses at moderate pressure are considered, γ_T will range between 20 and 200.

It is also possible to propagate a beam through a channel or near to the surface of a dielectric. In this case the threshold energy is greatly reduced. Substantial power² in the lower mm wavelength range can be obtained from devices driven by beams in the 100-200 KV range.

*Supported in part by the Air Force Office of Scientific Research, the Army Research Office, and the Office of Naval Research.

If the beam energy is increased, a device of this kind may also be useful at much shorter wavelengths. This follows from two basic considerations. The first is the scale length of the region over which the fields slowed by the dielectric resonator evanesce. It can be shown on very general terms that this is governed by:

$$\lambda \beta \gamma \quad \sim \quad b$$

where b is the scale length of the order of the beam diameter and beam-wave velocity synchronism is assumed. When b is a fraction of a millimeter, $\beta \gamma$ in the 2-20 range place λ in the far infrared part of the spectrum.

In calculating the gain in the short wavelength region, a non-collective approach may be adopted. A field with a component directed along the beam is assumed to exist. This produces a modulation current and the stimulated emission is the result of the work done by the beam back on the field. It is most convenient to express this as a reciprocal quality factor

$$\frac{1}{Q_b} \equiv \frac{R_e}{2\omega \mathcal{E}} \left[\int_{\text{beam}} \mathbf{j} \cdot \mathbf{E}^* dV \right]$$

where \mathcal{E} is the energy stored in the whole resonator, \mathbf{E} and \mathbf{j} are the electric field and the modulation current, and ω is the angular frequency of the emitted radiation. When $1/Q_b < 0$, gain is positive.

The gain expression can be placed in a relatively general form. If we assume that the beam may be regarded as monoenergetic at the wavelength of interest ($\lambda > L\delta\gamma/(\beta\gamma)^3$, L -resonator length) we can show:

$$\frac{1}{Q_b} = \frac{1}{(\beta\gamma)^3} \frac{I}{I_0} \frac{L^3 |E_z|^2}{8\pi\epsilon} \frac{\bar{n}}{n_0} \frac{\partial}{\partial \theta} \frac{(1 - \cos\theta)}{\theta^2}$$

where $\theta = (kv - \omega)L/v$ is the relative transit angle, and current, I , have been measured in units of $I_0 = ec/r_0$ ($r_0 = e^2/mc^2$). The terms in the expression which involve the field component in the beam direction and the stored energy are of the order of $L^2/\text{mode area}$, times a factor which is specifically dependent on the resonator. In addition, an effective relative beam density \bar{n}/n_0 is obtained from the transverse dependence of the fields. Typical designs for short wavelength devices and the results of recent experiments will be discussed.

References.-

1. Stimulated Cerenkov Radiation, in Advances in Electronics and Electron Physics, Vol. 58 (Academic Press, 1982).
2. A High Power Cerenkov Maser, with S. Von Laven, J. Branscum, J. Golub, and R. Layman, Appl. Phys. Lett., to be published September 1982.

Space-charge-Cerenkov and cyclotron-Cerenkov instabilities in an electron-beam dielectric system

William B. Case and Robert D. Kaplan
Grinnell College, Grinnell, Iowa 50112

John E. Golub and John E. Walsh
Dartmouth College, Hanover, New Hampshire 03755

(Received 6 June 1983; accepted for publication 21 December 1983)

A relativistic electron beam propagating along a constant magnetic field has four normal modes: the slow and fast space charge and the slow and fast cyclotron modes. When propagating through a dielectric where the beam velocity is greater than the velocity of light in the dielectric, the slow modes may become unstable. We call these the space-charge-Cerenkov and cyclotron-Cerenkov instabilities. In this paper we use the cold fluid model in the small signal limit to obtain a general dispersion relation for propagation at an arbitrary direction with respect to the magnetic guide field. This describes both of the above instabilities as special cases. This result is then generalized to include the effects of a thermal spread. Implications for possible application for generation or amplification of microwaves, where the beam passes near the dielectric, are also considered. We conclude that the cyclotron-Cerenkov instability is a strong candidate for the short wavelength microwave regime.

PACS numbers: 41.70. + t, 52.35.Py, 52.60. + h, 85.10.Ka

I. INTRODUCTION

A relativistic electron beam propagating along a constant magnetic field has four normal modes of oscillation.¹ Two of these are longitudinal oscillations and do not depend on the presence of an external field. These are negative energy (or slow) and positive energy (or fast) space-charge waves. The two remaining normal modes are transverse in character and do depend on the applied magnetic field. These are the slow and fast cyclotron waves. All modes are shown in Fig. 1.

For propagation in the vacuum, all four modes are stable. If the electron beam propagates through a dielectric medium, however, a slow wave may become unstable. Extensive theory has been developed to describe the exponential growth of the slow space-charge wave.²⁻⁶ Such growths occur only for beam velocities greater than the speed of light in the dielectric, and are therefore called Cerenkov instabilities.

In this paper we present a general theory which describes both the space-charge and cyclotron interactions. A derivation of the general dispersion relation is given in Sec. II, excitation of the slow space-charge wave is discussed in Sec. III, and a similar discussion of the slow cyclotron⁷ is given in Sec. IV. The special case of excitation of waves for an unmagnetized beam is presented in Sec. V. A warm beam version of this analysis is presented in Sec. VI. Finally, a comparison and discussion of implications for physical systems, where the beam cannot pass through the dielectric, is given in Sec. VII.

II. DERIVATION OF THE GENERAL DISPERSION RELATION

We consider an infinite, isotropic medium characterized by a dielectric constant ϵ . The dielectric is immersed in a constant magnetic field B_0 which we take to be along the z axis. An electron beam with velocity $\mathbf{v} = v_0 \hat{e}_z$, where \hat{e}_z is the

unit vector in the z direction, passes through the medium. We treat the beam as an infinite, cold plasma of electrons neutralized by a fixed ion background. Finally, we introduce an electromagnetic wave propagating through the beam-dielectric system at some angle θ to the z axis. The electric and magnetic fields associated with the wave are treated as perturbations to the system. We use a linearized, cold fluid theory and consider the small signal limit. The system is shown in Fig. 2.

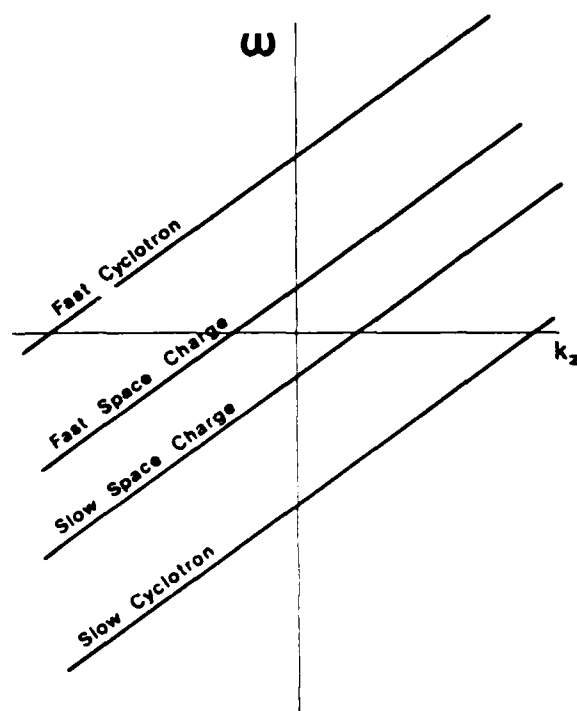


FIG. 1. Normal modes of an electron beam in a magnetic guide field.

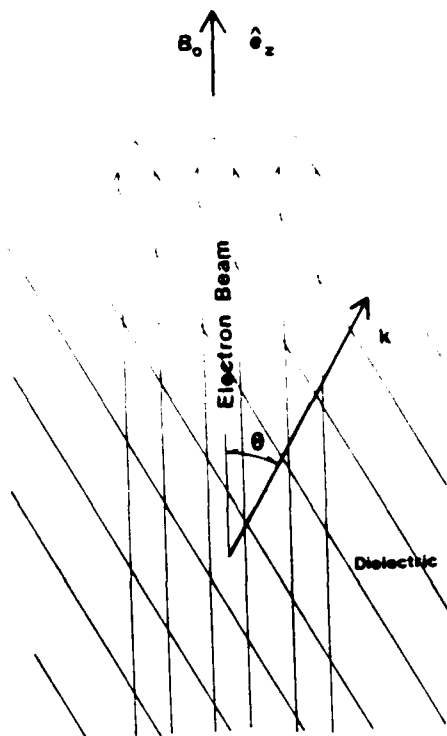


FIG. 2. Electron beam—magnetic field—dielectric system.

We begin by calculating the force on an element of the electron fluid due to the perturbation. The resulting equations of motion are solved to give the perturbed beam velocity. Specifically,

$$F = \frac{d(\gamma m \mathbf{v}_T)}{dt} = -e(\mathbf{E} + \mathbf{v}_T \times \mathbf{B}_T/c), \quad (1)$$

where $\gamma \equiv [1 - v_T^2/c^2]^{-1/2}$ is the usual relativistic factor. The subscript T is introduced to indicate total values as opposed to the first order perturbation to be introduced through linearization in the next step. We linearize these equations and consider components transverse and parallel to the magnetic field. The transverse component of the first order velocity then satisfies the following relation:

$$\begin{pmatrix} \frac{d}{dt} & \Omega/\gamma \\ -\Omega/\gamma & \frac{d}{dt} \end{pmatrix} \mathbf{v}_1 = -\frac{e}{m\gamma} (\mathbf{E}_1 + \mathbf{v}_0 \times \mathbf{B}_1/c), \quad (2a)$$

where $\Omega/\gamma = eB_0/\gamma mc$ is the cyclotron frequency. The axial component of perturbed velocity obeys:

$$\frac{dv_z}{dt} = -\frac{e}{m\gamma^3} E_z. \quad (2b)$$

The first order electric and magnetic fields are coupled through Faraday's law. Fourier transforming and making use of the explicit dependence on r and t , the equations of motion become:

$$\begin{pmatrix} \omega' & i\Omega/\gamma \\ -i\Omega/\gamma & \omega' \end{pmatrix} \mathbf{v}_1 = -\frac{ie}{mr} \times \left[\hat{e}_z \left[E_z \left(1 - \frac{v_0 k_z}{\omega} \right) + E_r \frac{v_0 k_1}{\omega} \right] + \hat{e}_r E_z \left(1 - \frac{v_0 k_z}{\omega} \right) \right], \quad (3a)$$

$$\omega = \frac{-eE}{m\gamma^3} \quad (3b)$$

where $\omega = \omega - k_z v_0$ is the frequency shift due to the zeroth order beam motion $\mathbf{k} = k_z \hat{e}_z + k_1 \hat{e}_r$ is the wave vector and is taken, without loss of generality, to lie in the x - z plane. Boundary conditions, introduced by finite transverse dimensions, are expected to fix k_z in a physical system. Solving for \mathbf{v} in terms of \mathbf{E} ,

$$\mathbf{v} = \frac{ie}{m} \begin{bmatrix} \frac{-\omega'^2}{\gamma\omega\omega'^2} & \frac{i\omega'\Omega}{\gamma^2\omega\omega'^2} & -\frac{v_0 k_1 \omega'}{\gamma\omega\omega'^2} \\ \frac{-i\omega'\Omega}{\gamma^2\omega\omega'^2} & \frac{-\omega'^2}{\gamma\omega\omega'^2} & \frac{-iv_0 k_1 \Omega}{\gamma^2\omega\omega'^2} \\ 0 & 0 & -\frac{1}{\gamma^3\omega'^2} \end{bmatrix} \mathbf{E}, \quad (4)$$

where $\omega'^2 = \omega'^2 - (\Omega/\gamma)^2$.

Next, we solve the equation of continuity to compute the perturbed density:

$$n = n_0 \mathbf{k} \cdot \mathbf{v} / \omega'. \quad (5)$$

Combining Eqs. (4) and (5) we can express the perturbed current density solely in terms of the electric field:

$$\mathbf{j} = \sigma \cdot \mathbf{E},$$

where

$$\sigma = \frac{ie^2 n_0}{m} \begin{bmatrix} \frac{\omega'^2}{\gamma\omega\omega'^2} & \frac{-i\omega'\Omega}{\gamma^2\omega\omega'^2} & \frac{v_0 k_1 \omega'}{\gamma\omega\omega'^2} \\ \frac{i\omega'\Omega}{\gamma^2\omega\omega'^2} & \frac{\omega'^2}{\gamma\omega\omega'^2} & \frac{iv_0 k_1 \Omega}{\gamma^2\omega\omega'^2} \\ \frac{v_0 k_1 \omega'}{\gamma\omega\omega'^2} & \frac{-iv_0 k_1 \Omega}{\gamma^2\omega\omega'^2} & \frac{v_0^2 k_1^2}{\gamma\omega\omega'^2} + \frac{\omega}{\gamma^3\omega'^2} \end{bmatrix} \quad (6)$$

We will use this current density as a source term in Maxwell's equations. Combining the curl equations, we find that the self-consistent fields are governed by

$$\left[\left(\frac{\epsilon\omega^2}{c^2} - k^2 \right) I + \frac{4\pi i\omega}{c^2} \sigma + \mathbf{k}\mathbf{k} \right] \mathbf{E} = 0, \quad (7)$$

where I denotes the unit tensor. Substituting Eq. (6) and choosing the nontrivial solutions, we arrive at the dispersion relation:

$$\det \left\{ \begin{bmatrix} \frac{\epsilon\omega^2}{c^2} - k_z^2 & 0 & k_1 k_z \\ 0 & \frac{\epsilon\omega^2}{c^2} - k^2 & 0 \\ k_1 k_z & 0 & \frac{\epsilon\omega^2}{c^2} - k_1^2 \end{bmatrix} + \frac{\omega_p^2 \omega}{c^2} \times \begin{bmatrix} \frac{-\omega'^2}{\gamma\omega\omega'^2} & \frac{i\omega'\Omega}{\gamma^2\omega\omega'^2} & \frac{-v_0 k_1 \omega'}{\gamma\omega\omega'^2} \\ \frac{-i\omega'\Omega}{\gamma^2\omega\omega'^2} & \frac{-\omega'^2}{\gamma\omega\omega'^2} & \frac{-iv_0 k_1 \Omega}{\gamma^2\omega\omega'^2} \\ \frac{-v_0 k_1 \omega'}{\gamma\omega\omega'^2} & \frac{iv_0 k_1 \Omega}{\gamma^2\omega\omega'^2} & \frac{-v_0^2 k_1^2}{\gamma\omega\omega'^2} - \frac{\omega}{\gamma^3\omega'^2} \end{bmatrix} \right\} = 0, \quad (8)$$

$$\text{where } \omega_p^2 = \frac{4\pi e^2 n_0}{m}$$

After considerable algebra, this becomes⁸

$$\begin{aligned} & \frac{\epsilon\omega^2}{c^2} \left(\frac{\epsilon\omega^2}{c^2} - k^2 \right)^2 \\ & - \frac{1}{\omega'^2} \left(\frac{\omega_p^2}{\gamma^2} \right) \left(\frac{\omega^2}{c^2} \right) \left(\frac{\epsilon\omega^2}{c^2} - k^2 \right) \left(\frac{\epsilon\omega^2}{c^2} - k_z^2 \right) - \frac{1}{\omega'^2} \left[\left(\frac{\omega_p^2}{\gamma} \right) \left(\frac{\omega^2}{c^2} \right) \left(\frac{\epsilon\omega^2}{c^2} - k^2 \right) \left[k_z^2 (\epsilon\beta^2 - 1) + \frac{2\epsilon\omega'^2}{c^2} \right] \right. \\ & \left. - \left(\frac{\omega_p^2}{\gamma c} \right) \left(\frac{\omega^2}{c^2} \right) \left[k_z^2 (\epsilon\beta^2 - 1) + \frac{\epsilon\omega'^2}{c^2} + \frac{(\epsilon\omega^2 - k_z^2)}{\gamma^2} + \frac{(\epsilon\omega^2 - k^2)}{\gamma^2} \right] + \left(\frac{\omega_p^2}{c^2 \gamma} \right) \frac{\omega^2}{\gamma^2} \right] = 0. \end{aligned} \quad (9)$$

This dispersion relation describes the normal modes of the coupled system. It is exact to within the limitations of the linear, cold fluid theory.

When ω_p is small, this relation will yield solutions very similar to the $\omega_p = 0$ (no beam) case except when the denominators ω'^2 or ω''^2 are small. As we will show, these cases lead to instabilities and we will refer to them as the space-charge-Cerenkov instability and the Cyclotron-Cerenkov instability, respectively. Although Eq. (9) can be solved by numerical methods, we first want to consider the distinct regimes where the ω'^2 pole or the ω''^2 pole dominates.

III. SPACE-CHARGE-CERENKOV INSTABILITY

As discussed at the end of the previous section, we seek solutions where $\omega_p \ll \omega$ and assume that ω' is sufficiently small so that the $1/\omega'^2$ term is negligible compared with the $1/\omega'^2$ term. In this limit Eq. (9) becomes

$$\epsilon \left(\frac{\epsilon\omega^2}{c^2} - k^2 \right) - \frac{1}{\omega'^2} \left(\frac{\omega_p^2}{\gamma^2} \right) \left(\frac{\epsilon\omega^2}{c^2} - k_z^2 \right) \approx 0. \quad (10)$$

When no interaction is present, the solutions are given by $\omega = \pm ck/\sqrt{\epsilon}$ for the free wave and $\omega = v_0 k_z \pm \omega_p/\gamma^{1/2}$ for space-charge waves. The interaction is maximum near synchronism where both the relations are approximately obeyed, as indicated in Fig. 3.

Hence, we set

$$\omega = \frac{ck}{\sqrt{\epsilon}} + \Delta_\pi \quad (11)$$

and

$$\omega' = \Delta_\pi.$$

Implicit in this condition is the assumption that $v_0 > c/\sqrt{\epsilon}$, and one can easily show that the system is stable if this condition does not hold. Equation (10) now becomes

$$\Delta_\pi^3 = \frac{\omega_p^2 c^2 \left(\frac{\epsilon\omega^2}{c^2} - k_z^2 \right)}{2\epsilon^2 \gamma^3 \omega}. \quad (12)$$

This has a real solution:

$$\Delta_\pi = \left[\frac{\omega_p^2 c^2 \left(\frac{\epsilon\omega^2}{c^2} - k_z^2 \right)}{2\epsilon^2 \gamma^3 \omega} \right]^{1/3}, \quad (13a)$$

and a pair of complex solutions:

$$\Delta_\pi = \left[\frac{\omega_p^2 c^2 \left(\frac{\epsilon\omega^2}{c^2} - k_z^2 \right)}{2\epsilon^2 \gamma^3 \omega} \right]^{1/3} \left(\frac{-1 \pm i\sqrt{3}}{2} \right). \quad (13b)$$

The upper sign describes an unstable mode with an exponential growth rate of

$$\begin{aligned} \omega_i &= \frac{\sqrt{3}}{2} \left[\frac{\omega_p^2 c^2 \left(\frac{\epsilon\omega^2}{c^2} - k_z^2 \right)}{2\epsilon^2 \gamma^3 \omega} \right]^{1/3} \\ &= \frac{\sqrt{3}}{2} \left[\frac{\omega_p^2 \omega (\epsilon\beta^2 - 1)}{2\epsilon^2 \gamma^3 \beta^2} \right]^{1/3}. \end{aligned} \quad (14)$$

When the plasma frequency is expressed in terms of the beam current (I), the Alfvén current ($I_0 = mc^3/e \sim 17$ KA) and the beam radius (a)

$$\omega_p^2 = 4 \left(\frac{I}{I_0} \right) \frac{c^2}{\beta a^2}, \quad (15)$$

the spatial gain may be written

$$\begin{aligned} \alpha_i &= \frac{\omega_i}{c\beta} \\ &= \frac{\sqrt{3}}{2a\beta\gamma} \left[\left(\frac{2}{\beta\epsilon^2} \right) \left(\frac{I}{I_0} \right) \left(\frac{a\omega_k}{c} \right) \left(\frac{\gamma^2 - 1}{\gamma^2} \right) \right]^{1/3}, \end{aligned}$$

where $\beta = v_0/c$, $\omega_k = ck_z = ck/\sqrt{\epsilon}$, and $\gamma_R \equiv \epsilon/(\epsilon - 1)$.

Once we have a value for ω_i , we must substitute it into Eq. (9) to check our assumption of the dominance of the

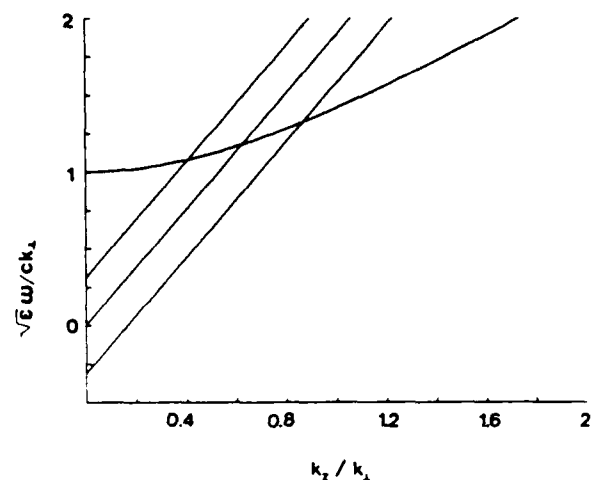


FIG. 3 Dispersion relations for the electron beam, and for the free electromagnetic modes in the dielectric. Synchronism occurs when the dispersion relations cross. The dispersion relations shown here are for a small plasma frequency hence the fast and slow space-charge modes coincide. The relations given are for $\epsilon = 4$, $k_1 = 2\pi \text{ cm}^{-1}$, $B_0 = 5 \text{ kg}$, and $\gamma = 3$.

$1/\omega'^2$ term over the $1/\omega''^2$ term. If our original assumption is to hold, we find we must add the requirement $\omega''/\omega' \Omega^2 \ll 1$. This is equivalent to assumption Ω sufficiently large and may be thought of as the infinite B limit.

In order to understand the mechanism of this instability we must return to the derivation of Eq. (9). We would obtain Eq. (10) had we used a conductivity tensor σ with only a nonvanishing σ_{xx} element given by $ie^2 n_e \omega / m \gamma^3 \omega'^2 = i\omega_p^2 \omega / 4\pi \gamma^2 \Delta_c^2$. That is, the instability depends only on j_z arising from E_z . When the relative phases of n and v_z are examined using Eqs. (4), (5), and (13) we find that they are out of phase by $4\pi/3$ for the growing mode. This means that the average mechanical kinetic energy of the beam has been reduced, since more electrons are traveling slower than the initial velocity v_0 than faster. This is called a negative energy wave since the amplitude increases as the mechanical energy decreases. This decrease in mechanical energy density appears as electromagnetic energy density, as can be shown by direct calculation.

IV. CERENKOV-CYCLOTRON INSTABILITY

We now seek solutions where the $1/\omega''^2$ term dominates the $1/\omega'^2$ term in Eq. (9). Again, adding the assumption $\omega \gg \omega_p$, Eq. 9 becomes

$$\epsilon \left(\frac{\epsilon \omega^2}{c^2} - k^2 \right) - \frac{1}{\omega''^2} \left(\frac{\omega_p^2}{\gamma} \right) \left[k_z^2 (\epsilon \beta^2 - 1) + \frac{2\epsilon \omega'^2}{c^2} \right] \approx 0. \quad (16)$$

The solutions when no interaction is present are given by $\omega = \pm ck/\sqrt{\epsilon}$ for the free waves, and $\omega = v_0 k_z \pm \Omega/\gamma$ for the cyclotron waves. As in the previous case, the interaction is maximized near synchronism when both relations are approximately obeyed. Hence, we set

$$\omega = ck/\sqrt{\epsilon} + \Delta_c,$$

$$\omega = v_0 k_z - \Omega/\gamma + \Delta_{cc},$$

where we have chosen the slow cyclotron mode. The fast mode may be shown to be stable by the same approach. Implicit in the assumption of synchronism is the condition $v_0 > c/\sqrt{\epsilon}$ and it can be shown that this mode becomes stable if this condition does not hold. Equation (16) now becomes

$$\Delta_{cc} = i\omega_I = \pm i \frac{\omega_p [c^2 k_z^2 (\epsilon \beta^2 - 1) + 2\epsilon \Omega^2 / \gamma^2]^{1/2}}{2\epsilon (\omega \Omega)^{1/2}}, \quad (17)$$

where the upper sign represents an unstable, exponentially growing mode. Using relation (15), the spatial gain for this process may be expressed as

$$\alpha_{cc} \equiv \frac{\omega_I}{c\beta} = \frac{[c^2 k_z^2 (\epsilon \beta^2 - 1) + 2\epsilon \Omega^2 / \gamma^2]^{1/2}}{[a^2 \epsilon^2 \beta^3 \omega \Omega]^{1/2}} \left(\frac{I}{I_0} \right)^{1/2}. \quad (18)$$

We must now examine the relative magnitudes of the terms in Eq. (9) using our result given in Eq. (13). Such analysis reveals that the neglected terms are indeed small if

$$\frac{\omega_p \omega'^{1/2}}{\beta \gamma \Omega^{1/2}} \ll 1. \quad (19)$$

$$\frac{\gamma \omega_p \Omega^{1/2}}{\omega'^{1/2}} \ll 1.$$

This instability involves two distinct mechanisms. In the first case we set $k_\perp = 0$ and allow Eq. (18) to be dominated by the $2\epsilon \Omega^2 / \gamma^2$ term. Here, E_z , B_z , $\nabla \cdot \mathbf{j}$ and n are all zero. Figure 4 indicates the relative phases of E , B , and v_z . The force due to the $-e\mathbf{v}_\perp \cdot \mathbf{B}/c$ term converts the original motion in the z direction into the perpendicular plane. The E field then does work on the electrons converting the mechanical energy into microwave energy. The only other first order force term present is $-e\mathbf{v}_\perp \times \mathbf{B}_0/c$ which holds the electrons in the helical orbits.

In the other case, where the $c^2 k_z^2 (\epsilon \beta^2 - 1)$ term dominates, the largest component of \mathbf{j} is j_z . This is in turn due to the large value of n rather than v_z . The bunching mechanism is best understood using Fig. 5 and noting that the dominant part of \mathbf{v} (the first order perturbation of the velocity) is the cyclotron motion, which is perpendicular to B_0 . As one can see in the figure, when $k_\perp \neq 0$ there are regions where the charge density increases due to the variation of phase with x . This results in the large value of n .

Further investigation reveals that n and E_z are in phase. When one integrates over a whole cycle, more energy is extracted from the higher density of electrons when E_z is positive than is added to the reduced density when E_z is negative, and mechanical energy is converted to electromagnetic energy. This can also be shown by direct calculation.

As indicated earlier, Eq. (9) can be solved directly by standard numerical methods. These have been carried out keeping terms to order ω_p^2 and the results are given in Figs. 6 and 7. These are very much what one would expect based on the preceding analysis: peaks in ω_I at the points of synchronism with the space-charge and cyclotron modes.

V. INSTABILITIES IN AN UNMAGNETIZED BEAM

In this special case $B_0 = 0$ and $\omega' = \omega''$. If we also assume ω_p is small and the synchronism condition, Eq. (9) becomes

$$\Delta^2 = \frac{\omega_p^2 c^2 \left[(1 - \beta^2) \left(\frac{\epsilon \omega^2}{c^2} - k^2 \right) + (\epsilon \beta^2 - 1) k_z^2 \right]}{2\epsilon^2 \gamma \omega},$$

where one term has been dropped in anticipation of the smallness of the growth rate Δ . In this limit the space-charge-Cerenkov and cyclotron-Cerenkov instabilities have become degenerate. As in the earlier case [Eq. (12)] this has a real solution and a complex conjugate pair of solutions. The

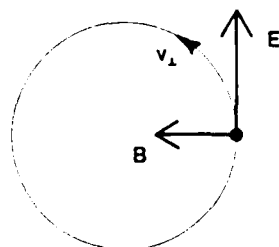


FIG. 4. Relative phase of E , B , and v_z for the $k_\perp = 0$ cyclotron instability

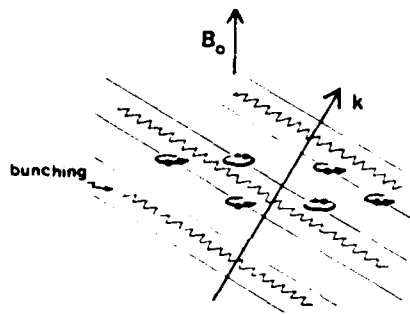


FIG. 5. Bunching mechanism for cyclotron instability for $k_z \neq 0$. By examining the relative phases of the cyclotron motions, one sees that the electron density is growing in the shaded region.

positive imaginary part by the complex solution is the growth rate and is given by

$$\omega_i = \frac{\sqrt{3}}{2} \left[\frac{\omega_p^2 \omega (\epsilon \beta^2 - 1) (\epsilon - 1)}{2 \epsilon^2 \gamma} \right]^{1/3}. \quad (20)$$

The spatial growth rate is given by

$$\alpha_i = \frac{\sqrt{3}}{2 a \beta} \left[2 \left(\frac{I}{I_0} \right) \left(\frac{\omega a}{c} \right) \left(\frac{\beta}{\gamma} \right) \left(\frac{1}{\gamma_R^2} \right) \left(\frac{\gamma^2 - 1}{\gamma^2 - 1} \right) \right]^{1/3}.$$

When this is compared with the space-charge-Cerenkov result given in Eq. (14) we obtain

$$\frac{\omega_i(B=0)}{\omega_i(B=\infty)} = (\beta^2 \gamma^2)^{1/3} [(\epsilon - 1)/\epsilon]^{1/3} > \epsilon^{-1/3}. \quad (21)$$

VI. EFFECTS OF THERMAL SPREAD OF THE BEAM

The effects of a thermal spread of the beam are included through the use of a multistreaming model.^{9,10} If $f_0(v)$ is the unperturbed velocity distribution, then $n_0 f_0(v) dv$ is the elec-

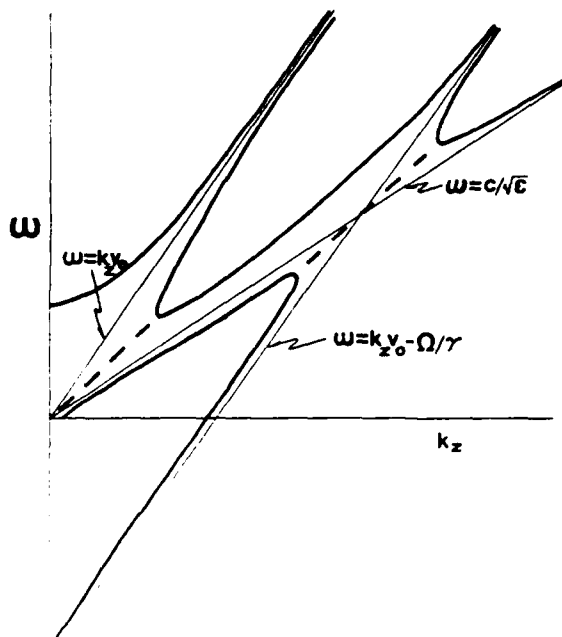


FIG. 6. To show the general character of the roots of Eq. (9), the real part of ω is plotted vs k_z . Heavy solid lines show real solutions and dashed lines are complex. The light lines are reference lines.

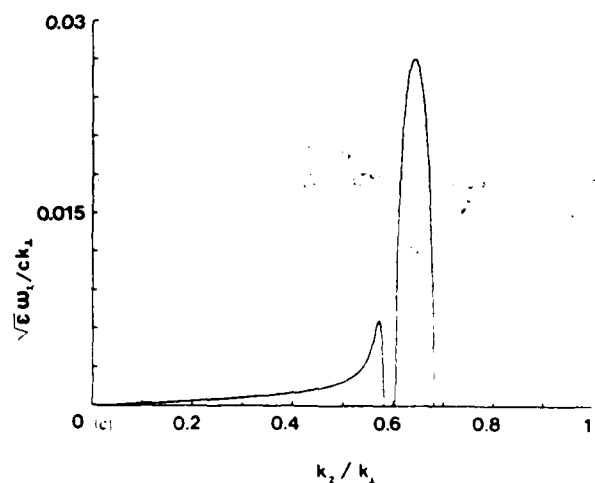
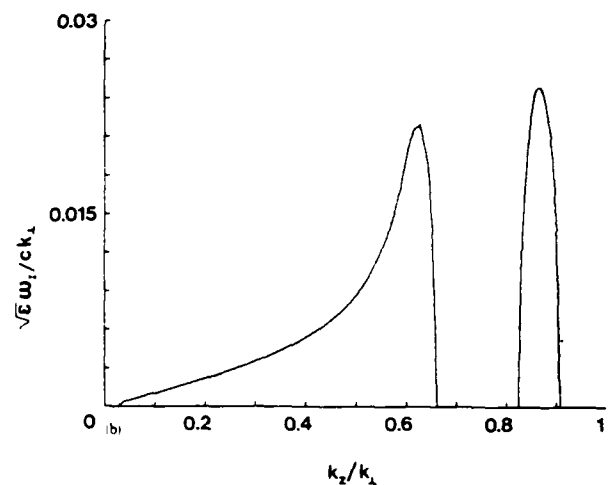
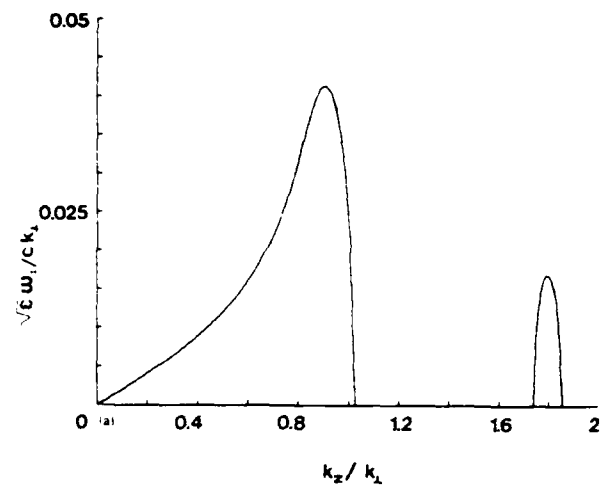


FIG. 7. Growth rates from Eq. (9), keeping terms to order ϵ^{-1} . In all cases $\epsilon = 4$, $B_0 = 5$ kg, spacing between conductors in the x direction $= b = 0.5$ cm (this fixes k_{\perp} at 2π cm⁻¹), and $\omega = 2\pi \times 10^7$ Hz (a is for $\beta = 1.5$, b is for $\beta = 3$, c is for $\beta = 10$).

tron density for the range v to $v + dv$. When this is incorporated in the plasma frequency of the cold beam [Eq. (9)] and the result integrated over v , we obtain

$$\epsilon \left(\frac{\epsilon \omega^2}{c^2} - k_z^2 \right) - \omega_p^2 \int f_0(v) \left\{ \frac{1}{\omega'^2} \left(\frac{1}{\gamma^2} \right) \left(\frac{\epsilon \omega^2}{c^2} - k_z^2 \right) + \frac{1}{\omega'^2} \left(\frac{1}{\gamma} \right) \left[k_z^2 (\epsilon \beta^2 - 1) + \frac{2\epsilon \omega'^2}{c^2} \right] \right\} dv = 0.$$

In this expression $\omega_p^2 \equiv 4\pi e^2 n_0/m$, and ω_p is assumed to be sufficiently small to allow us to neglect terms of order ω_p^4 and higher. For $f_0(v)$ we choose the Lorentzian distribution:

$$f(v) = \Delta \{ \pi [(v - v_0)^2 + \Delta^2] \}^{-1/2}.$$

If Δ is small, γ may be replaced by $\gamma_0 = [1 - (v_0/c)^2]^{-1/2}$ which is a constant during the integration. The integral is now analytic except for poles and the integral may be carried out by closing a contour at infinity. Since we seek growing solutions, we assume ω has a positive imaginary part, close the contour in the lower half plane, and use the residue theorem. We could close in the upper half plane, but this would require more algebra. This gives the warm beam dispersion relation:

$$\epsilon \left(\frac{\epsilon \omega^2}{c^2} - k_z^2 \right) - \omega_p^2 \left[\frac{\left(\frac{\epsilon \omega^2}{c^2} - k_z^2 \right)}{\gamma_0^2 k_z^2 \left(v_0 - \frac{\omega}{k_z} - i\Delta \right)^2} + \frac{k_z^2 [\epsilon(v_0 - i\Delta)^2 - 1] + \frac{2\epsilon}{c^2} [\omega - k_z(v_0 - i\Delta)]^2}{\{ [\omega - k_z(v_0 - i\Delta)]^2 - (\Delta/\gamma)^2 \}} \right] = 0. \quad (22)$$

We can again readily identify the first and second terms within the braces as the space-charge and cyclotron terms, respectively. This equation is solved numerically, and the results are presented in Fig. 8. It should be noted that for high γ the growth rate suffers very little for a given energy spread (where the spread is given as $\Delta\gamma/\gamma$ with $\Delta\gamma = (1 - [(v_0 + \Delta)/c]^2)^{-1/2} - \gamma_0$). At high γ a beam with a given spread will all be traveling at approximately c and all of the streams will generate waves which are in phase.

VII. COMPARISON OF THE DIFFERENT REGIMES AND IMPLICATIONS FOR MICROWAVE GENERATION AND CONCLUSIONS

When a relativistic electron beam passes through a dielectric, both the space-charge-Cerenkov and cyclotron-Cerenkov instabilities are expected to be present according to our theory (see Fig. 6-8). The geometry of a particular system will fix the perpendicular component of the wave vector k_\perp in both cases. Growth rates given in Eqs. (14) and (17) versus energy (γ) are shown in Fig. 9 for fixed values of ϵ , B_0 , k_\perp , and ω_p . With these variables fixed, the frequency of the waves generated vary along the curves and differ, somewhat, between the space-charge-Cerenkov and cyclotron-Cerenkov curves. This is most pronounced at lower energies as one would anticipate from Fig. 3. The growth rates for the space-charge-Cerenkov instability fall off at high γ while those for the cyclotron-Cerenkov instability remain high. By considering the growth rates at high γ [actually we need only

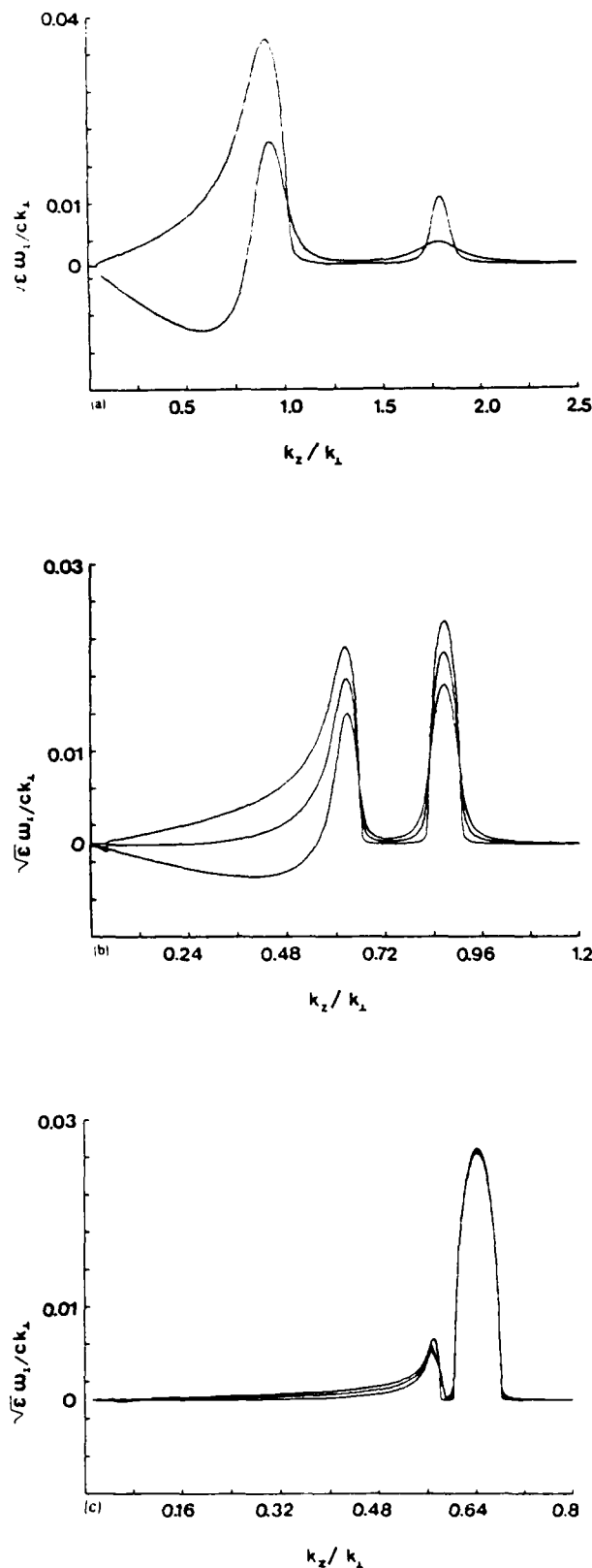


FIG. 8. Growth rates from Eq. (22) with $\epsilon = 4$, $B_0 = 5$ kg, $k_\perp = 2\pi \text{ cm}^{-1}$, and $\omega_p = 2\pi \times 10^9 \text{ Hz}$. (a) is for $\gamma = 1.5$ and $\Delta\gamma/\gamma = 0.01$ and 0.05 , the smaller value giving the greater growth. (b) and (c) are for $\gamma = 3$ and 10 , respectively. In both cases $\Delta\gamma/\gamma$ has been set equal to 0.01 , 0.05 , and 0.1 , the growth rates vary inversely with $\Delta\gamma/\gamma$, as expected.

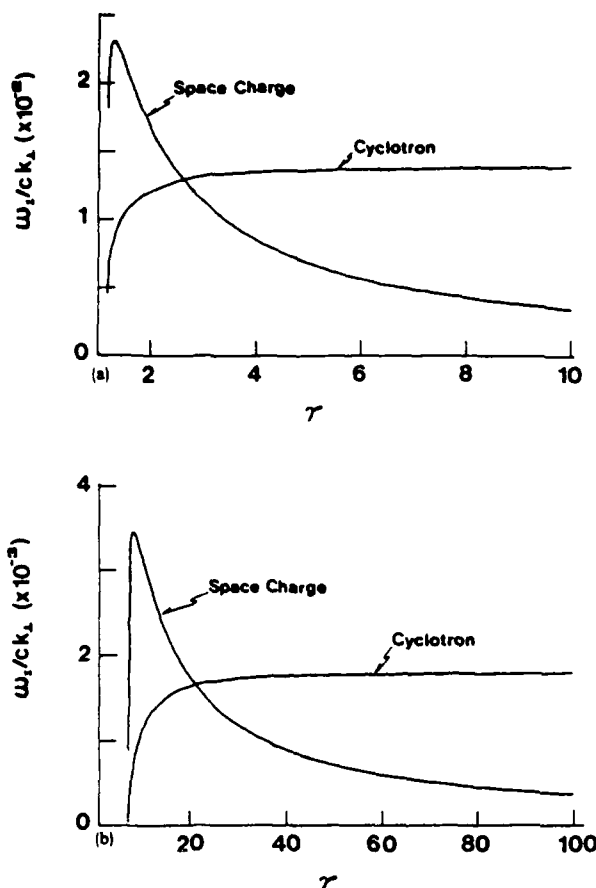


FIG. 9. Space-charge and cyclotron growth rates at synchronism vs γ . These are shown for fixed ϵ , B_0 , k_i , and ω_p . In (a) these values are $\epsilon = 3.78$ (quartz), $B_0 = 5$ kg, $k_i = 2\pi \text{ cm}^{-1}$ ($b = 0.5$ cm), and $\omega_p = 2\pi \times 10^9$ Hz; for (b) they are $\epsilon = 1.02$ (gas), $B_0 = 2.5$ kg, $k_i = 2\pi \text{ cm}^{-1}$ ($b = 0.5$ cm), and $\omega_p = 2\pi \times 10^9$ Hz.

$\omega^2 k_i^2 (\epsilon \beta^2 - 1) \gg 2\epsilon \Omega^2 / \gamma^2$, we see that Δ_{cc} approaches a constant while $\Delta_{sc} \propto \gamma^{-1}$. In the space-charge-Cerenkov case the motion is primarily in the z direction, a motion which the beam strongly resists as γ becomes large. In the cyclotron-Cerenkov case, however, the motion is perpendicular to z . The dependence of Δ_{cc} on the relativistic cyclotron frequency ($\Omega_{rel} = \Omega / \gamma$) is also relevant for this asymptotic dependence. This behavior will break down at very high γ , where the cyclotron pole at Ω / γ will approach the space-charge pole, spoiling the assumptions upon which Eqs. (14) and (17) are based. This same effect is responsible for the energy dependence of Eq. (21). Our interest in the high γ regime will be seen later. By considering the ratios of the cyclotron-Cerenkov and space-charge-Cerenkov growths in the high γ limit

$$\frac{\Delta_{cc}}{\Delta_{sc}} = \gamma \left(\frac{\omega_p c k_i}{4\epsilon \omega^{1/2}} \right)^{1/3} \frac{(\epsilon \beta^2 - 1)^{1/2}}{\Omega^{1/2}},$$

or

$$\frac{\Delta_{cc}}{\Delta_{sc}} = \gamma^{4/3} \left(\frac{(\epsilon \beta^2 - 1)^2}{4\epsilon} \right)^{1/3} \left[\frac{\omega_p \omega^{1/2}}{\gamma \beta \Omega^{1/2}} \right]^{1/2},$$

we see the higher plasma frequencies (current densities) favor the cyclotron-Cerenkov instability. It should be noted that the factor within the square brackets is the quantity

which must be much less than 1 in order for our approximations to hold. When the cube root is taken the quantity may well be close to 1 leaving the γ dependence to determine which growth rate is larger.

The issue of which instability dominates may not be as simple as comparing the growth rates. If the rates are comparable, the magnitude of the initial disturbance will be very significant in determining the final magnitude. A spatial increase in B_0 will give a cyclotron motion to the beam giving a sizable initial disturbance from which the cyclotron-Cerenkov instability can grow. Such considerations may lead one to conclude that the above comparison of growth rates tends to underestimate the strength of the cyclotron-Cerenkov signal.

In a physical system, the electron beam cannot propagate through the dielectric unless the dielectric is very weak such as a gas [see Fig. 9(b)], where the γ must be very large for synchronism. Hence, most actual experiments will consist of an electron beam passing through a hole in the dielectric. In such a system we have an electromagnetic wave propagating within the dielectric at a velocity of $c/\sqrt{\epsilon}$ with an exponential tail which extends into the hole. It is via this tail that the electron beam interacts with the electromagnetic wave. The e -folding length of the tail for a wave synchronous with the beam is given by

$$A = (v_\phi / \sqrt{1 - v_\phi^2}) \left(\frac{\lambda_{free}}{2\pi} \right) \approx \left(\frac{\gamma \beta}{2\pi} \right) \lambda_{free},$$

where λ_{free} is the wavelength of the wave when propagating through free space, v_ϕ the phase velocity of the wave in units of c , and the approximate result holds for large γ .

If we are to make efficient use of the beam we must maximize the overlap between the beam and this tail. Hence, we must have the entire beam within a few e -folding lengths of the dielectric. This problem is eased considerably by going to large values of γ , where the characteristic length of the tail may be many times the wavelengths in free space. Based on these considerations we see that the cyclotron is a strong candidate for microwave generation or amplification at short wavelengths. The gain per degree of overlap between the beam and waveguide mode (filling factor) is maximized in the regime where the overlap is greatest: high γ .

Another advantage of the high γ regime is the slight loss of growth resulting from thermal spread as noted in Sec. VI. This should also be true for the case where the beam passes near the dielectric.

It should also be noted that, when the beam passes near a dielectric, the dielectric becomes the waveguide whose modes are being excited and hence its dimensions will determine the resulting wavelength. Its transverse dimensions may be very small, since the beam need not pass through it, allowing very high frequencies to be generated. A detailed analysis of this system will be presented in a future paper, but the results are expected to be fairly similar to those given here. Based on these considerations, excitation of the cyclotron-Cerenkov instability by passing an intense high γ electron beam near a dielectric seems to present a promising way of generating or amplifying millimeter and submillimeter microwaves.

ACKNOWLEDGMENTS

We thank Professor Agnar Pytte for valuable discussions concerning this work and C. R. Boardman for checking many of the derivations. This work was supported in part by AFOSR Contract No. 82-0168.

- ¹W. H. Louisell, *Coupled Mode and Parametric Electronics* (Wiley, New York, 1961), Chap. 2. Note: the Synchronous Normal Modes, also discussed in this chapter, do not exist for a beam of infinite cross section.
- ²H. Lashinsky, "Cerenkov Radiation at Microwave Frequencies," in *Advances in Electronics and Electron Physics*, edited by L. Marton (Academic, New York, 1961), Vol. XIV, p. 265.

- ³J. E. Walsh, "Cerenkov and Cerenkov-Raman Radiation Sources," in *Physics of Quantum Electronics*, edited by S. Jacobs, M. Sargent, and M. Scully (Addison-Wesley, Reading, Mass., 1980), Vol. 7, p. 255.
- ⁴J. C. Jelley, *Cerenkov Radiation and its Applications* (Pergamon, London, 1958), p. 44.
- ⁵B. M. Bolotovskii, *Sov. Phys. Usp.* **4**, 781 (1962).
- ⁶K. L. Felch, Ph.D. thesis, Dartmouth, 1980.
- ⁷Some of these results have been presented earlier in, W. Case, J. Walsh, and D. Kapilow, *Bull. Am. Phys. Soc.* **25**, 959 (1980).
- ⁸G. G. Getmantsev and V. O. Rapoport, *J. Exp. Theoret. Phys. (USSR)* **38**, 1205 (1960) [*JETP* **11**, 871 (1960)]. These authors obtain a result which differs from Eq. (9) only by the absence of the relativistic factor γ in the plasma frequency. Equation (9) is the more correct result.
- ⁹J. M. Dawson, *Phys. Rev.* **118**, 381 (1960).
- ¹⁰T. H. Stix, *The Theory of Plasma Waves* (McGraw-Hill, New York, 1962), p. 114.

4. Abstracts of Work Presented at Scientific Meetings.

1. Far-Infrared Cerenkov Laser Experiments, J. Walsh, C. Shaughnessy, E. Garate et al.; 11th International Conference on Infrared and Millimeter Waves, 20-24 October, Pisa, Italy; 1986.
2. Cerenkov Free-Electron Laser Operation at Far-Infrared to Sub-millimeter Wavelengths, E. Garate, J. Walsh, B. Johnson and S. Moustazis, 8th Free-Electron-Laser Conference, Glasgow, Scotland, 1-5 September, 1986.
3. Amplification of a 406.1 μ m Laser Signal with a Cerenkov Free-Electron Laser Amplifier, E. Garate, C. Shaughnessy and J. Walsh, 8th FEL Conf., Glasgow.
4. Far-Infrared to Submillimeter-Wavelength Cerenkov FEL Operation, E. Garate, J. Walsh, C. Shaughnessy, B. Johnson and S. Moustazis, APS Division of Plasma Physics Conference, Baltimore, MD, November 1986.
5. Lower and Submm-Wavelength Cerenkov FEL, E. Garate, S. Moustazis, J.M. Buzzi, C. Rouille, J. Walsh and B. Johnson, APS Division of Plasma Physics Conf., 1986.
6. Mode-Locking of Langmuir Waves in a Beam-Driven Plasma, R. McCowan and J. Walsh, Bull. Am. Phys. Soc. 30, 1492 (1985).
7. A 100 μ m Cerenkov FEL Experiment, J. Walsh, B. Johnson, C. Shaughnessy, A. Renieri, G. Dattoli and G. Gallerano, Bull. Am. Phys. Soc. 30, 1549 (1985).
8. Cerenkov Amplifiers, J. Branscum, R. Layman, T. Buller and J. Walsh, Bull. Am. Phys. Soc. 29 1434 (1984).
9. Effect of Beam Quality on Cerenkov Gain, J. Walsh, B. Johnson, E. Garate and G. Dattoli, Bull. Am. Phys. Soc. 29, 1434 (1984).
10. Chaotic Behavior of Electron-Beam-Driven Waves, R. McCowan and J. Walsh, Bull. Am. Phys. Soc. 29, 1406 (1984).
11. Excitation of the Slow Cyclotron Wave by the Passage of a Superluminous Electron-Beam Near a Dielectric Slab, W. Case, R. Kaplan and J. Walsh, Bull. Am. Phys. Soc. 28, 1087 (1983).
12. Experimental Performance of a Cerenkov Maser at Lower-Mm Wavelengths, J. Walsh, E. Garate, T. Buller, R. Layman and D. Willey, Bull. Am. Phys. Soc. 28, 1089 (1983).

13. A Two-Stage Cerenkov Oscillator, J. Walsh, S. Von Laven, R. Layman, E. Garate and R. Cook, Bull. Am. Phys. Soc. 27, 1017 (1982).
14. A High-Power Cerenkov Microwave Source, S. Von Laven, J. Branscum, J. Golub, R. Layman and J. Walsh, IEEE International Conference on Plasma Science, 17-19 May, 1982.

Far-Infrared Cerenkov Laser Experiments

J. Walsh, C. Shaughnessy, E. Garate
Dartmouth College
Hanover, N.H. 03755

G. Dattoli, F. Ciocchi, A. Renieri,
A. Dipace, G.P. Gallerano, E. Sabia
ENEA
Frascati (Roma)
Italy

Recent experimental progress on Cerenkov laser development in the 100-1000 μm wavelength range will be reviewed. Devices driven by RF microtron accelerators and other types of electron beam generators will be described. Descriptions of various approaches to resonator design and the results of optical cold-testing will also be presented.

CERENKOV FREE ELECTRON LASER OPERATION AT FAR INFRARED TO SUB-MILLIMETER WAVELENGTHS

E. P. Garate, J. Walsh, C. Shaughnessy, B. Johnson
Department of Physics and Astronomy,
Dartmouth College, Hanover, N.H.
and
S. Moustazis
Laboratoire de Physique des Milieux Ionises,
Ecole Polytechnique, Palaiseau , France

The first time operation of a planar dielectric lined waveguide, driven by a dense ($n \sim 10^{12} \text{ cm}^{-3}$), mildly relativistic ($1.8 < \gamma < 3$) electron beam is reported. The interaction has produced voltage tunable radiation at wavelengths between $400 \mu\text{m}$ and 1 mm with an estimated power output of 200 KW at the 1 mm wavelength and 75 KW at the $500 \mu\text{m}$ wavelength, yielding efficiencies of $\sim .1\%$. Experimental results indicate very good agreement with the theoretically predicted output wavelength for operation on the TM_{01} mode of the dielectrically loaded waveguide.

This work was supported in part by U.S. A.R.O. contract DAAG29-85-K-0176, A.F. O.S.R. contract 82-0168 and DRET contract 86.028.

AMPLIFICATION OF A 496.1 μm LASER SIGNAL
WITH A
CERENKOV FREE ELECTRON LASER AMPLIFIER

E. P. Garate, C. H. Shaughnessy, J. E. Walsh
Department of Physics and Astronomy
Dartmouth College, Hanover, New Hampshire

A Cerenkov FEL has been successfully operated as a superradiant amplifier, yielding tunable output from 400 μm to 1 mm with electron beam energies less than 1.1 MeV.¹ We propose to amplify the 496.1 μm line of methyl fluoride from an optically-pumped far-infrared laser (FIR) with a Cerenkov FEL amplifier.

The collective linear gain is predicted to be about 1 dB/cm using a moderate current, cold electron beam. A prism will efficiently couple the linearly polarized FIR laser signal to the TM_{01} thin film waveguide mode. Direct measurement of the guide wavelength verifies the predicted dispersion of the mode.

A novel "bent waveguide" design for the amplifier is described in detail. The proposed coupling optics and detection scheme are presented.

Using electron beam energies of approximately 400 keV, the Cerenkov amplifier would be quite compact and capable of high repetition-rate pulsed operation. With the proper choice of dielectric film thickness, high output powers can be obtained at any of the wavelengths available from the optically-pumped FIR laser. In principle, the output linewidth should be comparably narrow.

This work is supported in part by U.S.A.R.O. contract DAAG29-85-K-0176 and A.F.O.S.R. contract 82-0168.

1. E. P. Garate, et. al. , to be published

Abstract Submitted for the Twenty-Eighth Annual Meeting
Division of Plasma Physics
November 3-7, 1986

Category Number and Subject 4.9 Coherent radiation generation

☐ Theory

☒ Experiment

Far Infrared to Submillimeter Wavelength Cerenkov F.E.L. Operation *

E.P. Garate, J. Walsh, C. Shaughnessy, B. Johnson, Dartmouth College
S. Moustazis, Ecole Polytechnique, (France)-- The first time operation of a rectangular, partially filled with dielectric waveguide driven by a dense ($n \sim 10^{12} \text{ cm}^{-3}$), mildly relativistic ($1.8 < \gamma < 3$) electron beam is reported. The interaction has produced voltage tunable radiation at wavelengths between $400 \mu\text{m}$ and 1 mm with an estimated power output of 200 KW at the 1 mm wavelength and 75 KW at the $500 \mu\text{m}$ wavelength, yielding efficiencies of $\sim .1\%$. Tuning curves will be presented for the measured output wavelength as a function of the electron accelerating voltage for the range 400Kv to 1.1Mv. Experimental results indicate very good agreement with the theoretically predicted output wavelength for operation on the TM_{01} mode of the dielectrically loaded waveguide.

*Supported in part by U.S.A.R.O. contract DAAG29-85-K-0176,
A.F. O.S.R. contract 82-0168 and DRET contract 86.028.

☐ Prefer Poster Session

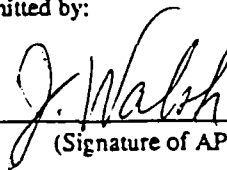
☒ Prefer Oral Session

☐ No Preference

Special Requests for Placement of
this Abstract: _____

Special Facilities Requested (e.g., movie
projector): _____

Submitted by:



(Signature of APS Member)

John Walsh

(Same Name Typewritten)

Dept. of Physics and Astronomy
Dartmouth College, Hanover, N.H.
(Address)

This form, or a reasonable facsimile, plus TWO XEROX COPIES, must be received by NO LATER THAN NOON,
Friday, July 18, 1986, at the following address:

Ms. Dana Richards
L-630
Lawrence Livermore National Laboratory
P. O. Box 5511
7000 East Avenue
Livermore, CA 94550
(415) 422-9858

Lower and Sub- mm Wavelength Cerenkov F.E.L.,

E. Garate, S. Moustazis, J. M. Buzzi, C. Rouille, Ecole Polytechnique (France), J. Walsh, B. Johnson, Dartmouth College*.---The interaction of a dense (10^{12} cm^{-3}), mildly relativistic electron beam ($1.8 < \gamma < 3$) with a cylindrical, dielectric loaded slow wave structure has produced tunable output radiation at 0.95-mm to 2-mm wavelengths. The estimated power output is 500 kw at the 2-mm wavelength and at least 10 kw at the 0.95-mm wavelength, giving a conversion efficiency of 0.5%. Tuning curves will be presented for the measured output wavelength as a function of the electron beam accelerating voltage for the voltage range 400 Kv to 1 Mv. The wavelength was measured using a grating spectrometer calibrated to operate in the 0.85-mm to 8-mm wavelength range. Results indicate very good agreement with the theoretically predicted output wavelength for operation on the TM_{01} mode of the dielectrically loaded waveguide.

* Supported in part by AFOSR grant #82-0168

Abstract Submitted
For the Twenty-Seventh Annual Meeting
Division of Plasma Physics
November 4-8, 1985

Category Number and Subject 1.1.11 Electron beam/plasma interactions

☐ Theory

☒ Experiment

Mode Locking of Langmuir Waves in a Beam Driven Plasma. R. B. McCowan, J. E. Walsh, Dartmouth College.* Longitudinal waves in a cylindrical magnetized plasma will mode lock when two electron beams of equal voltage and opposite direction are introduced into the plasma. One beam is generated by a heated cathode electron gun, the other beam is formed by reflecting the first from the endplate.

The primary effect of the two beam system is to symmetrize the dispersion relation for the beam driven waves; this allows high quality standing waves to exist in the plasma column. The beat frequencies between these standing waves will lock and force the waves to become equally spaced in frequency. When the phases of the modes are equal the signal measured on a loop antenna shows a pulsed output analogous to that of a mode locked laser¹.

The wave amplitudes are treated as coupled oscillators with nonlinear dissipation. Oscillators of this type are known to show entrainment phenomena². Theoretical and experimental results will be presented.

* This work is supported in part by AFOSR grant 82-0163

1 Hargrove, Fork and Pollack, Appl Phys Lett. v.8 1966

2 B. van der Pol, Proc IRE 22, 1934

☒ Prefer Poster Session

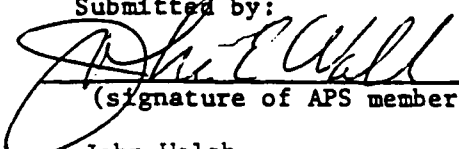
☐ Prefer Oral Session

☐ No Preference

☐ Special Requests for placement of this abstract:

☐ Special Facilities Requested (e.g., movie projector)

Submitted by:


(signature of APS member)

John Walsh

(same name typewritten)

Department of Physics

(address)

Dartmouth College, Hanover, N.H.

This form, or a reasonable facsimile, plus Two Xerox Copies must be received 03755
NO LATER THAN Noon, Friday, July 26, 1985, at the following address:

Division of Plasma Physics Annual Meeting
c/o Ms. Barbara Sarfaty
Princeton Plasma Physics Laboratory
P. O. Box 451
Princeton, New Jersey 08544

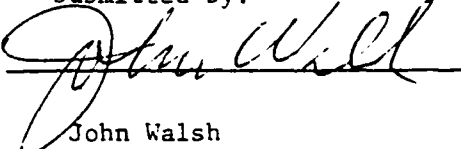
Abstract Submitted
For the Twenty-Seventh Annual Meeting
Division of Plasma Physics
November 4-8, 1985

Category Number and Subject 4.9.3 Free Electron Lasers

A 100 μ m Cerenkov FEL Experiment. J. WALSH,
B. JOHNSON, and C. SHAUGHNESSY, Dartmouth College*,
A. RENIERI, G. DATTOLI, and G. GALLERANO, E.N.E.A.
Frascati--A 100 μ m-wavelength, microtron-accelerator-driven, Cerenkov laser experiment is planned. The accelerator operates at an energy of 5 MeV and has a peak current of 2A in the micropulse. The beam is transported through a thin dielectric-film-loaded planar resonator which supports cylindrical-Gaussian modes and for the designed beam and resonator parameters, unity small-signal gain-per-pass can be achieved. Transport focus and positioning at the electron beam is accomplished with three-quadropole magnets, a positioning magnet and a solenoid. With the anticipated accelerator beam quality and transport channel parameters (energy spread and emittance), the monoenergetic beam approximation will apply and the expected efficiency is in the 1% range. A discussion of the design details and preliminary experimental results will be presented.

*Supported in part by AFOSR Grant 82-0168 and
ARO Grant DAAG29-83-K-0018.

Submitted by:


John Walsh

Department of Physics

Dartmouth College

Hanover, N.H. 03755

Abstract Submitted
For the Twenty-Sixth Annual Meeting
Division of Plasma Physics
October 29 to November 2, 1984

Category Number and Subject 4.9.3 Free Electron Lasers

☐ Theory

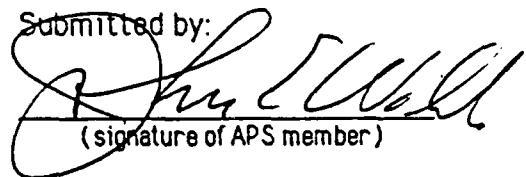
☒ Experiment

Cerenkov Amplifiers. J. Branscum, R. W. Layman, T. Buller and John Walsh, Dartmouth College*--Cerenkov oscillators and many other beam driven devices make use of cylindrically symmetric TM modes of a wave guiding structure. This class of mode may not be the one which is most convenient for input coupling in an amplifier, however, and for this reason a number of dielectric loaded structures which support linearly polarized modes have been investigated. Two which have been considered in detail are standard rectangular guides loaded with flat slabs of dielectric and flat plate quasioptical resonators loaded with thin dielectric films. The first of these supports two classes of mode usually denoted as LSE(M). These are closely related to the more familiar TE and TM modes. The second type of resonator will support a mode which is Hermite-Gaussian in the direction across the guide and cylindrical about an axis perpendicular to the plane of the resonator. The free mode dispersion curves and derivations of the Cerenkov gain in both the single particle and collective interaction limits will be discussed for both types of structure. Preliminary experimental data will also be presented.

* Supported in part by AFOSR grant #82-0168

- ☐ Prefer Poster Session
- ☐ Prefer Oral Session
- ☒ No Preference
- ☐ Special Requests for Placement of this abstract:
- ☐ Special Facilities Requested (e.g., movie projector)

Submitted by:


(signature of APS member)

JOHN WALSH
(same name typewritten)

Dartmouth College
(address)

Division of Plasma Physics Annual Meeting
c/o Ms. Barbara Sarfaty
Princeton Plasma Physics Laboratory
P. O. Box 451
Princeton, New Jersey 08544

Abstract Submitted
For the Twenty-Sixth Annual Meeting
Division of Plasma Physics
October 29 to November 2, 1984

Category Number and Subject 4.9.3 Free Electron Lasers

☒ Theory

☐ Experiment

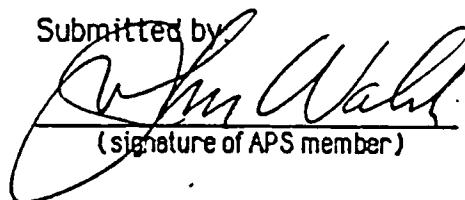
Effect of Beam Quality on Cerenkov Gain J. Walsh,
B. Johnson, Dartmouth College*, E. Gerate, Ecole Polytechnique,
G. Dattoli, ENEA (Frascati) -- Generalized beam quality parameters
which determine Cerenkov laser performance may be defined. These
are related to the relative energy spread, to the finite beam
emittance, and, in short pulse experiments, to the relative slippage
between the beam and the radiation. These parameters, together
with an expression for the relation between beam current density
and emittance¹, can be used to develop optimum expressions for
gain and other quantities. We will show that this argument, which
has already been used for Free Electron Lasers in the Compton
limit, can be extended to sources operating in the collective limit.
In this extension a relative beam strength parameter must also be
introduced. The resulting expressions will be used to establish
optimum parameters for Cerenkov amplifiers.

¹ "Lawson-Penner Limit and Single Passage Free Electron
Laser Performance", G. Dattoli, T. Letardi, J.M.J. Madey, and
A. Renieri, IEEE J - QE (1984).

* Supported in part by AFOSR grant #82-0168

- ☒ Prefer Poster Session
☐ Prefer Oral Session
☐ No Preference
☐ Special Requests for Placement
of this abstract:
☐ Special Facilities Requested
(e.g., movie projector)

Submitted by:


(signature of APS member)

JOHN WALSH

(same name typewritten)

Dartmouth College

(address)

Division of Plasma Physics Annual Meeting
c/o Ms. Barbara Sarfaty
Princeton Plasma Physics Laboratory
P. O. Box 451
Princeton, New Jersey 08544

Abstract Submitted
For the Twenty-Sixth Annual Meeting
Division of Plasma Physics
October 29 to November 2, 1984

Category Number and Subject 1.2 Nonlinear Waves and Instabilities

☐ Theory

☒ Experiment

Chaotic Behavior of Electron Beam Driven Waves.

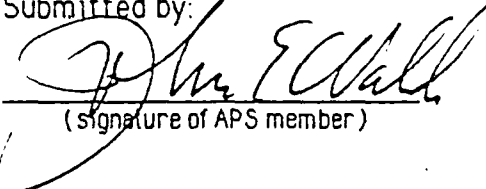
Robert McCowan and John Walsh, Dartmouth College*-- Chaotic behavior now appears to be a universal phenomenon in nonlinear systems. The present work is an attempt to observe chaotic behavior of longitudinal plasma modes in a beam plasma. The experiment consists of a strongly magnetized electron beam formed plasma column with an electron density of 10^9 to 10^{10} electrons/cm³. The plasma is probed with a second beam with voltages from 0 to 1000 volts, and currents from 0 to 30 mA. The purpose of this second beam is to drive natural modes of the bounded system unstable; the nature of these unstable waves is studied.

The behavior of unstable longitudinal waves in a bounded lossy system can be modelled using coupled van der Pol oscillators. Coupled nonlinear equations of this type show subharmonic bifurcations leading to chaos via the route described by Feigenbaum. Experimental and theoretical results will be presented.

*This work has been supported in part by AFOSR grant 82-0168.

- ☒ Prefer Poster Session
☐ Prefer Oral Session
☐ No Preference
☐ Special Requests for Placement
of this abstract:
☐ Special Facilities Requested
(e.g., movie projector)

Submitted by:


(signature of APS member)

JOHN WALSH

(same name typewritten)

Dartmouth College

(address)

Division of Plasma Physics Annual Meeting
c/o Ms. Barbara Sarfaty
Princeton Plasma Physics Laboratory
P. O. Box 451
Princeton, New Jersey 08544

Abstract Submitted
For the Twenty-fifth Annual Meeting
Division of Plasma Physics
November 7 to 11, 1983

Category Number and Subject 4.9 Coherent Radiation Generation

☒ Theory ☐ Experiment

Excitation of the Slow Cyclotron Wave by the
Passage of a Superluminous Electron Beam Near a
Dielectric Slab*, WILLIAM B. CASE and ROBERT D. KAPLAN,
Grinnell College, and JOHN E. WALSH, Dartmouth College.
We consider the excitation of the slow cyclotron wave
due to the interaction of a superluminous electron
beam passing near a dielectric slab. The analysis is
carried out by treating the electron beam as a cold
fluid which perturbs the degenerate polarization modes
of the electromagnetic waves in free space. The
resulting modes are then matched to the modes within
the dielectric producing a dispersion relation for the
system. When solved using numerical techniques, we
find exponential growths for the slow cyclotron mode
(Cyclotron-Cerenkov) as well as the usual slow space
charge mode (Space Charge-Cerenkov). If this system is
to be used for generation of submillimeter waves, one
must use high γ ($\gamma > 2\pi$) to guarantee good coupling.
In this regime the growth rate for the Cyclotron-
Cerenkov instability is greater than that for the
Space Charge-Cerenkov. Considerations of the effects
of thermal spread will also be given.

*Work supported in part by AFOSR Contract # 82-6108.

- ☒ Prefer Poster Session
☐ Prefer Oral Session
☐ No Preference
☐ Special Requests for placement
of this abstract:
☐ Special Facilities Requested
(e.g., movie projector)

Submitted by:

William B. Case
(signature of APS member)

William B. Case

(same name typewritten)
Grinnell College, Grinnell, Iowa

(address)

50112

This form, or a reasonable facsimile, plus *Two Xerox Copies* must be received
NO LATER THAN Noon, Friday, July 15, 1983, at the following address:

Division of Plasma Physics Annual Meeting
c/o Ms. Barbara Sarfaty
Princeton Plasma Physics Laboratory
P. O. Box 451
Princeton, New Jersey 08544

Abstract Submitted
For the Twenty-fifth Annual Meeting
Division of Plasma Physics
November 7 to 11, 1983

Category Number and Subject 4.9 Coherent Radiation Generation
.3 Free Electron Lasers

☐ Theory

☒ Experiment

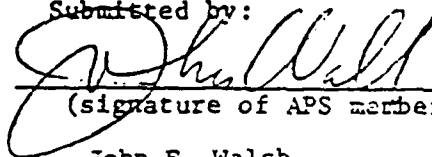
Experimental Performance of a Cerenkov Maser
at Lower mm Wavelengths. J. WALSH, E. GARATE,
T. BULLER, R.W. LAYMAN, R. COOK and D. WILLEY,
Dartmouth College*--Cerenkov Masers have achieved
hundred-KW power levels in the middle-mm range and
outputs in excess of ten KW in the lower-mm region¹.
Substantial output levels, on higher order cavity
modes, have also been obtained at wavelengths below
1 mm. However, the typical single-stage high power
output pulse is often considerably less than the
electron beam pulse length. In the longer wavelength
range, two-stage, oscillator-amplifier operation has
been used to increase the pulse length and the
overall stability of the output. The results of
attempts to extend this concept to shorter wavelength
will be discussed. In addition, resonator design
criteria for fundamental mode operation in the 1-mm
wavelength range and preliminary experimental results
will be presented.

1. A High Power Cerenkov Maser Oscillator, S. Von
Laven et al., Appl. Phys. Lett. 41(5), 408 (1982).

*Supported in part by AFOSR Contract # 82-0168 and
ARO Contract # DAAG29-83-K-0018.

- ☐ Prefer Poster Session
☐ Prefer Oral Session
☒ No Preference
☐ Special Requests for placement
of this abstract:
☐ Special Facilities Requested
(e.g., movie projector)

Submitted by:


(signature of APS member)

John E. Walsh

(same name typewritten)

Physics Department, Dartmouth

(address)

Hanover, N.H.

This form, or a reasonable facsimile, plus Two Xerox Copies must be received
NO LATER THAN Noon, Friday, July 15, 1983, at the following address:

03755

Division of Plasma Physics Annual Meeting
c/o Ms. Barbara Sarfaty
Princeton Plasma Physics Laboratory
P. O. Box 451
Princeton, New Jersey 08544

Abstract Submitted
For the Twenty-Fourth Annual Meeting
Division of Plasma Physics
November 1 to 5, 1982

4.8 Microwave Generation

Category Number and Subject: ~~1.12 Electron beam/plasma interactions.~~

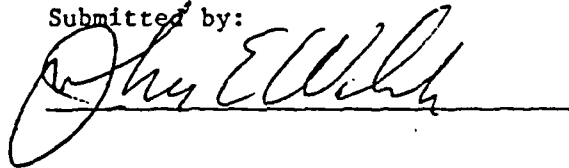
Experimental

A Two-Stage Cerenkov Oscillator, J.E. WALSH, S. VON LAVEN, R.W. LAYMAN, E. GARATE and R. COOK, Dartmouth College*--Recently¹, 100 KW levels of output power have been obtained in Cerenkov oscillator experiments. The device, which has been described in more detail elsewhere, consists of a pulse transformer-generated, 100-200 KV, 10-20 A, 1 μ sec beam pulse, a dielectric-loaded guide, and a variety of output coupling structures. The output power levels indicate that the beam is nearly 100% modulated during its passage through a 10 cm-long resonator. This in turn suggests that enhancement of the output power could be obtained if the now bunched beam is passed through a second resonator which is weakly coupled to the first, and whose phase velocity is lower than that of the first resonator. Such a device is similar to a multi-cavity klystron or a velocity-tapered traveling wave tube. A theoretical analysis and results of experimental investigation of this concept will be presented.

1. A High Power Cerenkov Maser Oscillator, S. Von Laven, J. Branscum, J. Golub, R. Layman and J. Walsh, Appl. Phys. Lett., Sept. 1, 1982, to be published.

Supported in part by AFOSR Contract # 82-0168 and ARO Contract # DAAG-29-79-C-0203-A01.

Submitted by:



John Walsh

No preference for
Session

Dartmouth College, Hanover, N.H. 03755

17-19 May, 1982

A High Power Cerenkov Microwave Source.* S. Von Laven, J. Branscum, J. Golub, R. Layman and J. Walsh, Dartmouth College. An electron beam-driven dielectric-lined waveguide has produced 30-100 kilowatts of coherent radiation over an octave band on the TM01 mode of the waveguide. Operation on the TM02 mode has been realized as well. Impedance mismatches at the ends of the liner section provide a reflected signal, which undergoes amplification during successive passes.

This work employs a pulsed, 1-40 ampere beam of 100-250 keV electrons directed along the axis of a dielectric-lined circular waveguide¹.

The pulse duration is about four microseconds. Quartz ($\epsilon_p=3.78$), stycast ($\epsilon_p=5$), and boron nitride ($\epsilon_0=4.2$) liners of several thicknesses have been employed.

For most dielectric liners used, the fundamental output frequency is near the frequency at which the phase velocity of the TM01 mode is synchronous with the beam. Data will be presented for several liners in 12.5 mm diameter waveguide. A large systematic error is noted for the case of the 3 mm quartz liner. A surface charge build-up on the quartz is suspected of decelerating the beam to velocities synchronous with the observed output. The problem nearly disappears for 2 mm quartz. The longitudinal electric field associated with the 1 mm liner geometry is too weak to give good coupling for moderate beams.

The output power is found to increase as the square of the beam current in the 1-10 ampere range for the 2 mm quartz liner, again in 12.5 mm diameter waveguide. In a separate, absolute measurement with the same liner geometry, a 12-ampere, 115 kilovolt beam generated 30 kilowatts of radiation at 50 GHz. Powers up to 100 kilowatts were obtained at lower frequencies for 3 mm thick boron nitride in the 12.5 mm diameter waveguide. Power is often sufficient to cause atmospheric breakdown in X-band waveguide.

The range of frequencies obtainable on a single mode has reached nearly an octave. In some of the 12.5 mm diameter waveguide experiments and in a 9.5 mm waveguide experiment, it has been possible to suppress the TM01 mode and observe coupling to the TM02 mode. Frequencies between 100 and 120 GHz have been attained. The power is probably less than that obtainable on the TM01 mode, but still significant. Lower levels of output have been observed through a 200-GHz filter with the 2 mm quartz liner, 12.5 mm waveguide.

Discrete cavity modes are observed rather than a continuous waveguide spectrum. The Q of the liner section itself is an important parameter. Reduced reflectivity at either end raises the voltage threshold for output.

*Work supported by AFOSR Contract # 77-3410D.

¹K.L. Felch, K.O. Busby, R.W. Layman, D. Kapilow and J.E. Walsh, Appl. Phys. Lett. 38, 601 (1981).

END

1-87

DTIC